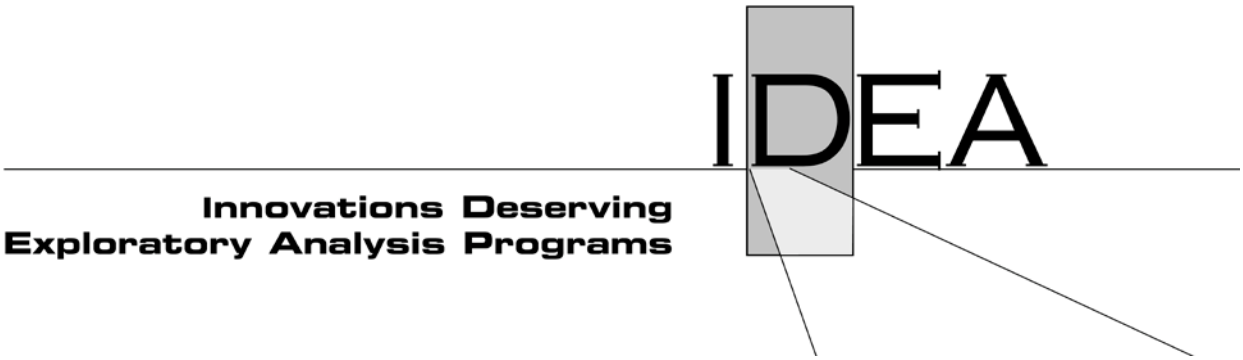

NCHRP IDEA Program

Measuring Concrete Permeability with CHIP

Final Report for
NCHRP IDEA Project 232

Prepared by:
M. Tyler Ley
Niloofer Parestegari
Amir Behravan
Dan Cook
Qinang Hu
Oklahoma State University

September 2023

NATIONAL ACADEMIES Sciences Engineering Medicine

TRB TRANSPORTATION RESEARCH BOARD

Innovations Deserving Exploratory Analysis (IDEA) Programs Managed by the Transportation Research Board

This IDEA project was funded by the NCHRP IDEA Program.

The TRB currently manages the following three IDEA programs:

- The NCHRP IDEA Program, which focuses on advances in the design, construction, and maintenance of highway systems, is funded by American Association of State Highway and Transportation Officials (AASHTO) as part of the National Cooperative Highway Research Program (NCHRP).
- The Safety IDEA Program currently focuses on innovative approaches for improving railroad safety or performance. The program is currently funded by the Federal Railroad Administration (FRA). The program was previously jointly funded by the Federal Motor Carrier Safety Administration (FMCSA) and the FRA.
- The Transit IDEA Program, which supports development and testing of innovative concepts and methods for advancing transit practice, is funded by the Federal Transit Administration (FTA) as part of the Transit Cooperative Research Program (TCRP).

Management of the three IDEA programs is coordinated to promote the development and testing of innovative concepts, methods, and technologies.

For information on the IDEA programs, check the IDEA website (www.trb.org/idea). For questions, contact the IDEA programs office by telephone at (202) 334-3310.

IDEA Programs
Transportation Research Board
500 Fifth Street, NW
Washington, DC 20001

The project that is the subject of this contractor-authored report was a part of the Innovations Deserving Exploratory Analysis (IDEA) Programs, which are managed by the Transportation Research Board (TRB) with the approval of the National Academies of Sciences, Engineering, and Medicine. The members of the oversight committee that monitored the project and reviewed the report were chosen for their special competencies and with regard for appropriate balance. The views expressed in this report are those of the contractor who conducted the investigation documented in this report and do not necessarily reflect those of the Transportation Research Board; the National Academies of Sciences, Engineering, and Medicine; or the sponsors of the IDEA Programs.

The Transportation Research Board; the National Academies of Sciences, Engineering, and Medicine; and the organizations that sponsor the IDEA Programs do not endorse products or manufacturers. Trade or manufacturers' names appear herein solely because they are considered essential to the object of the investigation.

NCHRP IDEA PROGRAM

COMMITTEE CHAIR
KEVIN PETE
Texas DOT

MEMBERS
FARHAD ANSARI
University of Illinois at Chicago
AMY BEISE
North Dakota DOT
NATANE BRENNFLECK
California DOT
JAMES "DARRYLL" DOCKSTADER
Florida DOT
ERIC HARM
Consultant
SHANTE HASTINGS
Delaware DOT
PATRICIA LEAVENWORTH
Massachusetts DOT
TOMMY NANTUNG
Indiana DOT
DAVID NOYCE
University of Wisconsin, Madison
A. EMILY PARKANY
Vermont Agency of Transportation
TERESA STEPHENS
Oklahoma DOT
JOSEPH WARTMAN
University of Washington

AASHTO LIAISON
GLENN PAGE
AASHTO

FHWA LIAISON
MARY HUIE
Federal Highway Administration

TRB LIAISON
ILONA KASTENHOFER
Transportation Research Board

IDEA PROGRAMS STAFF
CHRISTOPHER HEDGES
Director, Cooperative Research Programs
WASEEM DEKELBAB
Deputy Director, Cooperative Research Programs
SID MOHAN
Associate Program Manager
INAM JAWED
Senior Program Officer
PATRICK ZELINSKI
Senior Program Officer
Mireya Kuskie
Senior Program Assistant

EXPERT REVIEW PANEL
PATRICIA LEAVENWORTH, *Massachusetts DOT*
WALT PETERS, *Oklahoma DOT*
MARIA MASTEN, *Minnesota DOT*
ROBERT SPRAGG, *FHWA*

MEASURING CONCRETE PERMEABILITY WITH THE CHIP

NCHRP IDEA Program Final Report

For the period July 2021 through September 2023

IDEA Project NCHRP-232

Prepared for

The NCHRP IDEA Program
Transportation Research Board
National Academies of Sciences, Engineering, and Medicine

by

M.Tyler Ley, Niloofar Parastegari, Amir Behravan, Dan Cook, Qinang Hu

Oklahoma State University

9/30/2023

TABLE OF CONTENTS

EXECUTIVE SUMMARY

This project is a continuation of a previous IDEA project (NCHRP-199) that developed a prototype device to determine the permeability of hardened concrete using X-rays to measure the penetration of a tracer. In this follow-on project, the current instrument sample holder is being improved so that larger samples can be scanned. This new sample holder will also be able to find the locations of previous scans to allow the investigation of many different sample orientations, saving operator time and making the device easier to use. The software for the device will also be improved to make it easier and faster for the user. The work goes on to describe the three case studies that use the developed technology. The first case study focuses on the effectiveness of wet curing and how different curing lengths impact the Diffusion coefficient (D_{ic}) of the concrete. Next, the performance of silane sealers is measured in field cores. Finally, the long-term change in the D_{ic} is measured with mixtures that contain different amounts and types of fly ash. The work goes on to improve the reliability of the test by increasing the number of angles to evaluate the sample and the width of the analysis area. Finally, work was done to decrease the length of the testing time from 28 days to roughly 6h. The test is accelerated by using a current to drive the tracer through the concrete. More research is needed to use this with a wide range of materials to investigate the effectiveness, but the results look promising. An overview of the test method is provided with the suggested wording that is useful for developing a testing standard.

IDEA PRODUCT

Concrete infrastructure is a significant investment for State Highway Agencies (SHAs). Because of this, these concrete structures must have a long service life. The permeability of concrete is critical in the durability of concrete. This work improves an existing device called the CHIP (**ch**ecking **i**on **p**enetration). The CHIP can determine the permeability of concrete with a non-destructive, practical, fast, safe, and easy to use, which employs X-ray to image the penetration of outside salts into the concrete. The CHIP can be used to evaluate the permeability of concrete during mixture designs, construction, or for concrete structures in service. This ability to rapidly and economically determine the permeability of concrete and predict the service life is a powerful tool for SHAs.

SHAs do not regularly use direct measurements to determine their concrete permeability because current methods are slow, labor-intensive, and expensive. Instead, SHAs use indirect methods with electron flow within the concrete to estimate the permeability. Unfortunately, there are many variables that impact the accuracy of electrically based methods. If SHAs could use a direct measurement technique that is accurate and rapid, then critical permeability information could be obtained about the concrete during mixture design evaluation, construction, or when planning the maintenance of existing structures. The CHIP can fill this need by providing a direct permeability measurement in 28 days with minimal human time and can be completed on 20 mm diameter cores. The device would enable SHAs to set in-place performance permeability specifications for their concrete. Also, the CHIP could be used on existing concrete structures to find their permeability and determine the remaining service life. In addition, the CHIP can be used to compare the effectiveness of different sealers or repair materials used in concrete.

CONCEPT AND INNOVATION

The amount of connected pores within concrete, also known as the permeability, influences the ability of outside fluids to penetrate into the concrete. The permeability is important for freeze-thaw, carbonation, corrosion, alkali-silica reaction, and sulfate attack performance of concrete. Therefore, the harder it is for these outside chemicals to penetrate through the concrete, the lower the permeability and the longer the service life. Unfortunately, the current methods of directly measuring the permeability of concrete are expensive and time-consuming. However, if a rapid test method could be developed that could provide a direct measurement of the permeability, then this would be a powerful tool to ensure that low permeability concrete is used in the mixture design and after consolidation and curing. This tool could also be useful to determine the permeability and service life of existing structures.

The CHIP (**ch**ecking **i**on **p**enetration) device was designed as a non-destructive, practical, fast, safe, and inexpensive approach to measuring the rate of fluid penetration into paste, mortar, or concrete. The current version of this direct permeability measurement takes 28 days and has been completed by taking a 20 mm core and capturing an X-ray image or radiograph of the concrete before and after a tracer or electron-dense liquid penetrates through the sample. FIGURE 1 shows the Prototype CHIP developed from previous NCHRP IDEA funding.

FIGURE 1 CHIP prototype

Most life-cycle analysis models for concrete use the D_{ic} to predict the service life. The CHIP can determine the D_{ic} by using X-rays to image the sample before and after being ponded with a tracer for seven days. By subtracting these two images, the penetration of the tracer can be seen. An example of the results is shown in FIGURE 2(a). Quantitative measurements of the tracer can be found by using the intensity values from the images and by using standards to change this information into concentration. These standards are concrete with known amounts of tracer added. These standards do not need to be used again

as they indicate the amount of signal in the machine to the amount of tracer present in the sample. The final results are shown in FIGURE 2(b). These concentrations quantify the amount of the tracer that has penetrated into the concrete. From this graph, a D_{ic} can be found.

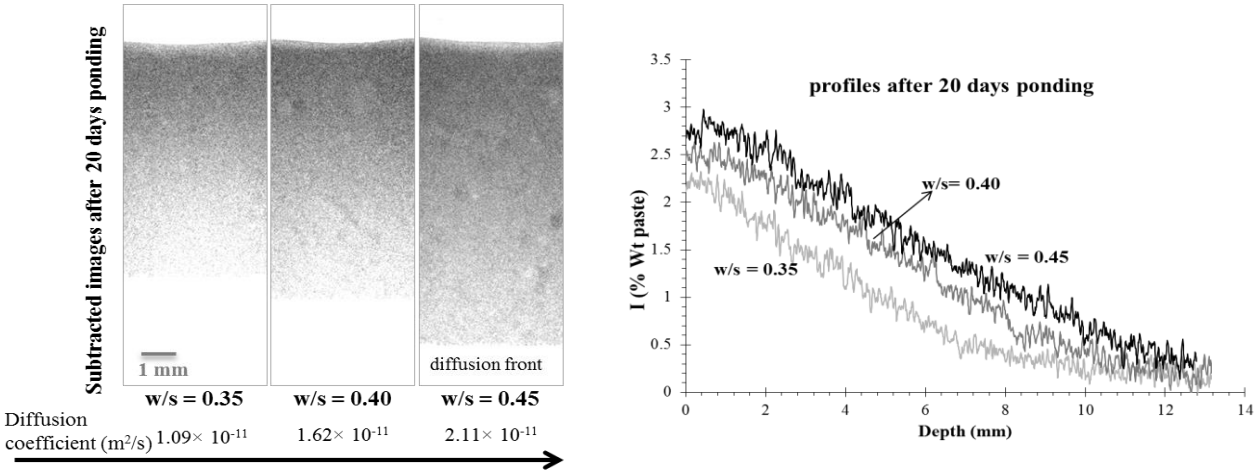

(a) (b)

FIGURE 2 (a) ion penetration and (b) ion concentration profile of three mixtures with different w/s and diffusion coefficients.

Although a functioning prototype was created in the previous NCHRP work, improvements in the functionality of the software and equipment, reduction in the length of the test, and development of new case studies to show the usefulness of the device are needed to gain the confidence of SHAs, FHWA, and AASHTO.

This research is the first step in establishing a product to give SHAs an inexpensive and powerful tool that could be used in the laboratory and field to directly determine the permeability of their concrete infrastructure. This device could be used to evaluate concrete mixture designs and compare construction practices such as finishing, consolidation, and curing. This means that the measurements would be from the in-place properties of the concrete. This could warn the owner if a problem were occurring during the construction process. In addition, this method could be used to compare the effectiveness of different repair materials or the use of surface sealers to prolong the service life of the concrete. This would allow SHAs greater insight into the performance of their existing and new concrete structures.

The following are the tasks from the project. These tasks were used as the headings of the sections in this report.

Task 1 Kickoff meeting with expert panel

Task 2 Redesign X-ray Prototype

Task 3 Rewrite Software

Take 4 Case Studies

Task 5 Stage 1 Report and Progress

Task 6 Evaluate the Repeatability of the test

Task 7 Develop Accelerated Test Method

Task 8 Prepare the Final Report.

INVESTIGATION

A kickoff meeting was held on February 1, 2021, over Zoom. The research panel was in attendance. The panel consisted of Patricia Leavenworth – Massachusetts DOT; Walt Peters – Oklahoma DOT; Maria Masten – Minnesota DOT; and Robert Spragg - FHWA. The meeting provided an update on the work plan, a description of the work performed to date, and an outline of the work to be done in the future. There was good feedback from the committee, and several improvements were made to the testing plan.

Redesign X-ray Prototype

The previous sample holder was manually controlled by a human, and it is outlined in FIGURE 3. This sample holder is simple and easy to operate, but it requires attention to detail when operating. As part of this project, a new sample holder was developed that is more user-friendly, has capabilities to make the scans easier for the operators, and can allow larger samples to be investigated.

This larger and more sophisticated sample holder is shown in FIGURE 4, FIGURE 5, and FIGURE 6. FIGURE 4 shows a concrete sample mounted on the sample holder with the X-rays coming from one direction and a detector on the other side of the sample. The sample holder uses precise motors and displacement devices to move in three different ways. These movements are shown with x, y, and θ. Details of the overview of the motors, power supply, driver, and controller are shown in FIGURE 5 and FIGURE 6. This system provides precise movement to 0.05 mm accuracy. This is 4x more accurate than what was done in the previous testing setup.

This sample holder allows the sample to move vertically, horizontally, and to rotate. The vertical and horizontal movement allows the sample to be aligned in a known spot in a repeatable manner. This is helpful because a user can have the CHIP scan a known location and then remove the sample so that they can scan others, and then several days later, they can place the sample back in the instrument and send it to the same location as it did for the first scan.

This movement can also allow a larger area of the sample to be scanned. This is shown in FIGURE 7. This larger scan can be created by taking an image in one location, moving the camera to another location with the vertical and horizontal motors, and then taking another image. This can be repeated, and the images can be joined together to form one large composite image. Based on the current X-ray strength of the CHIP, the largest size that is practical to be scanned is 3" diameter or a 3" thickness. This could be increased in size with higher-power X-ray transmitters; however, this is outside of the scope of this project.

The rotation sample holder is helpful to allow the sample to be scanned from many different angles. This provides a larger number of measurements from a single sample. By using more angles than one, we

can average out the non-homogeneous sections within the sample. For example, the KI solution does not penetrate the aggregates, and so this provides an area with high concentrations of KI in the paste and low concentrations in the aggregate. However, in the measurement, we just want to find the average performance of the sample, as this is what we care about in our final concrete structures. Using observations from a larger number of angles provides a better estimate of the average. Work on this project shows that observations from five angles with about 40^{o} between each image provide the same reliability as taking images from a larger number of angles. This is discussed more in Task 6. All of these efforts make the test more accurate and also reduce the amount of time and effort to complete a scan.

FIGURE 3 The existing sample holder used in the CHIP

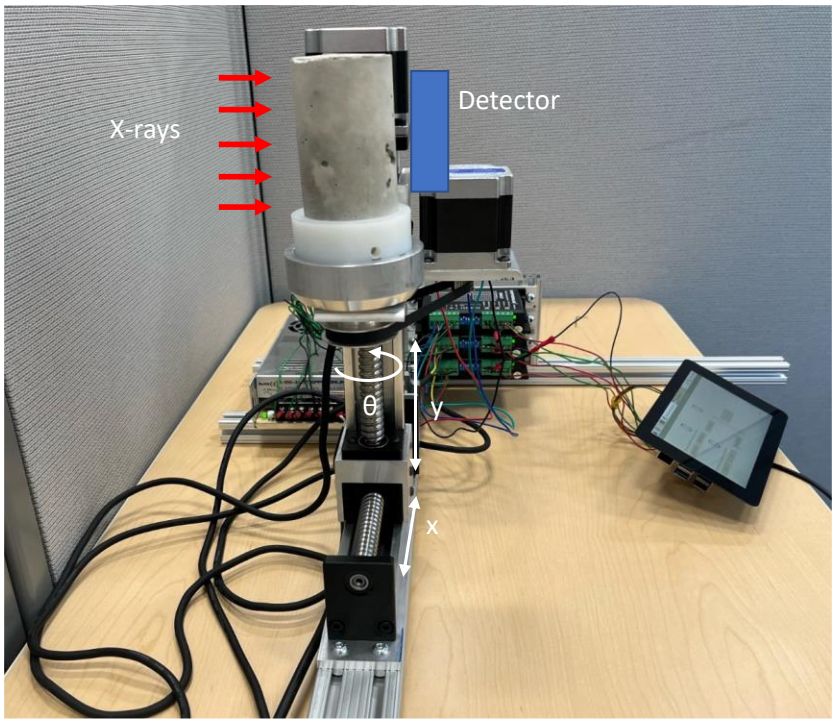

FIGURE 4 An overview of the new sample holder for the CHIP

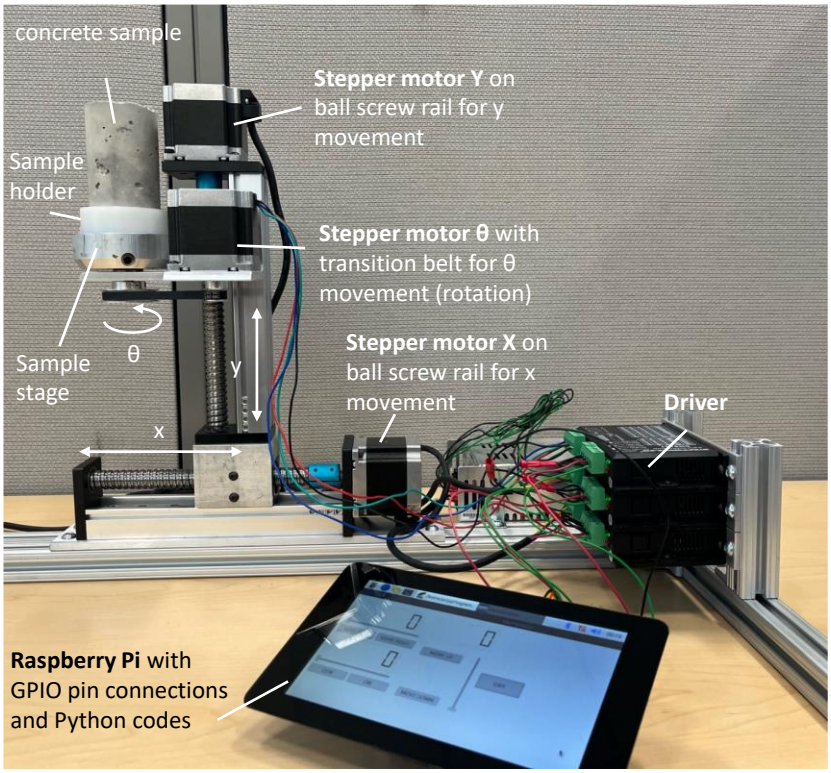

FIGURE 5 An elevation view showing the new sample holder with details about the motors used, the driver, and the controller.

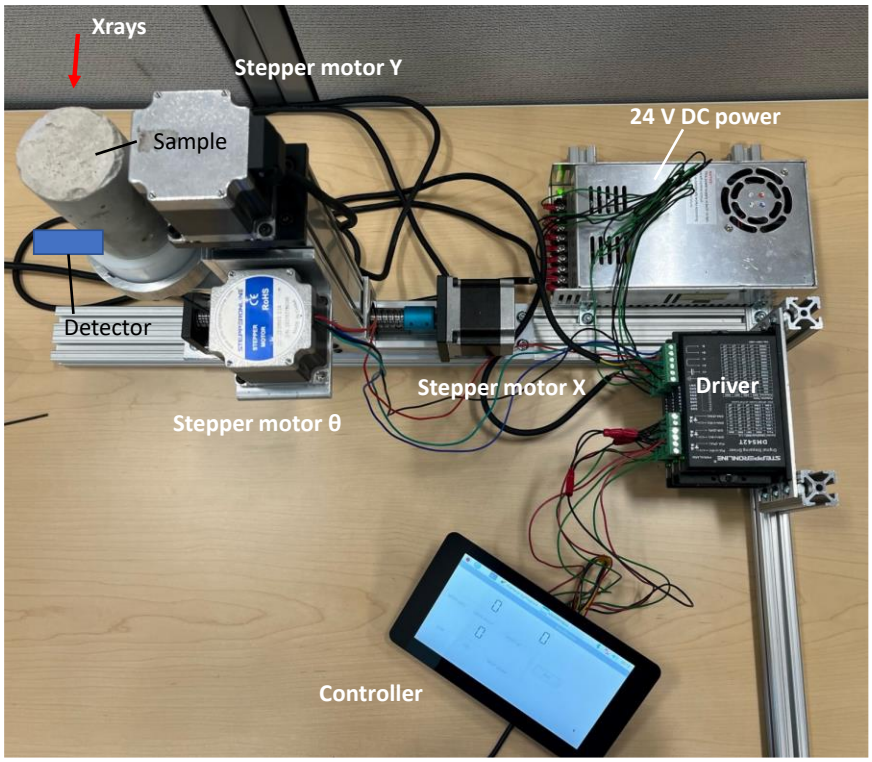

FIGURE 6 A top view of the new sample holder showing the motors, driver, power supply, and controller.

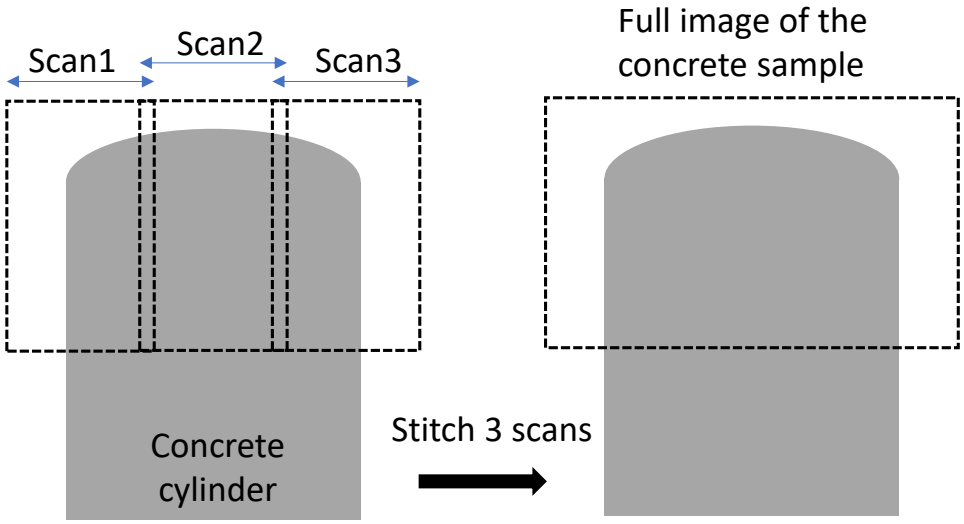

FIGURE 7 Using several smaller scans to create a single image of a sample.

Update software

The original version of the CHIP used three angles and a narrow strip to determine the D_{ic} of the samples. These methods were sufficient for paste or mortar where the sample was largely homogenous, but these needed to be improved for concrete samples. To improve the measurements in concrete, the CHIP sample holder was modified to take images from a larger number of angles. Also, instead of using a narrow strip, the software started to use the data from the entire sample. The raw scan and the average gray value from the scan are shown in FIGURE 8. The average gray value is a measurement of how much energy passes through the sample. Because the sample is a cylinder, there is a different amount of material at the edges than at the center. This means that more energy is passing at the edges. As the tracer penetrates the concrete, this also changes the amount of energy that is absorbed. To make the analysis simpler, the first version of the CHIP only measured at the center of the cylinder because the thickness did not significantly vary. This limited the amount of sample that was investigated.

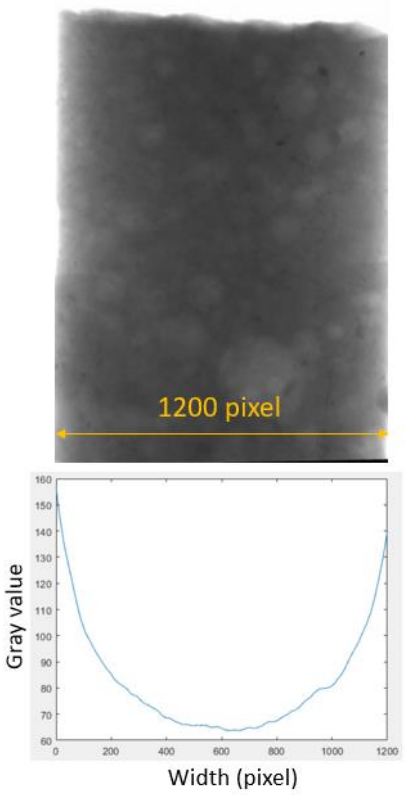

FIGURE 8 Gray value vs. width

To address this problem, the gray value was normalized based on the geometry of the sample so that the gray value is constant. This is shown in FIGURE 9. This allows the entire diameter of the sample to be used in the experiments. By using the entire width of the sample and by using 12 different angles in the

measurement, the coefficient of variation was improved from 0.48 to 0.25 for concrete samples. This is a significant improvement in the reliability of the measurement.

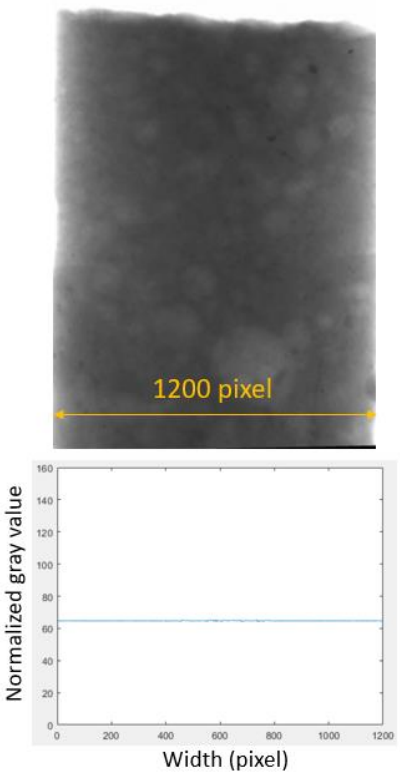

FIGURE 9 Normalized gray value vs. width.

The first version of the software must be run separately for each angle of each sample. Therefore, if four samples were investigated from a bridge deck and 12 angles were used for each sample, then the code was used 48 separate times. This was time consuming and also created an opportunity for human error. The code was modified to allow all of the images to be analyzed simultaneously.

Because the captured images were not perfectly aligned, the first version of the code required the user to manually rotate and shift the sample so that they were in the same location. This required some user training to be sure the correct points were chosen, and also it was time consuming. The new version of the software does all of this automatically. This again improves the repeatability, reduces operator time, and improves the usefulness of the equipment.

Case studies

Quantifying the impact of wet concrete on a bridge deck

Curing is an important process in producing durable concrete. Wet curing is often used when concrete needs to be the most resistant to deterioration. The purpose of wet curing is to provide continuous moisture

to the fresh cement-based system to promote hydration (1,2). As a result, wet curing can improve the porosity, permeability, strength, shrinkage, and creep of the resulting concrete (3–9). While there are many benefits to applying wet curing to concrete, there are also challenges because wet curing requires significant labor, and it is not clear when wet curing should be placed on the surface of the fresh concrete.

The goal of this case study is to investigate the influence of wet curing applied at different times in different evaporative environments to determine the allowable delay in applying the wet curing on the surface before the properties of the concrete are compromised. This work examines the performance in evaporation rates between 0.03 lbs/ft2/h and 0.17 lbs/ft2/h. These evaporation rates are commonly observed in practice but are not the highest evaporation rates that can be measured. This research purposely focused on lower evaporation rates as they would show the most potential to delay the application of wet curing. A nomograph predicting the evaporation rates based on different weather conditions is shown in FIGURE 10. The evaporation rates investigated are shown. The curing methods evaluated include wet curing applied to the surface with no delay or continuous wet curing, wet curing applied with a delay between 2h and 10h, and samples with no curing applied to the surface or air curing. When wet curing is applied to the surface with no delay, it will be called "continuous wet curing." The samples that were not cured will be called "air curing."

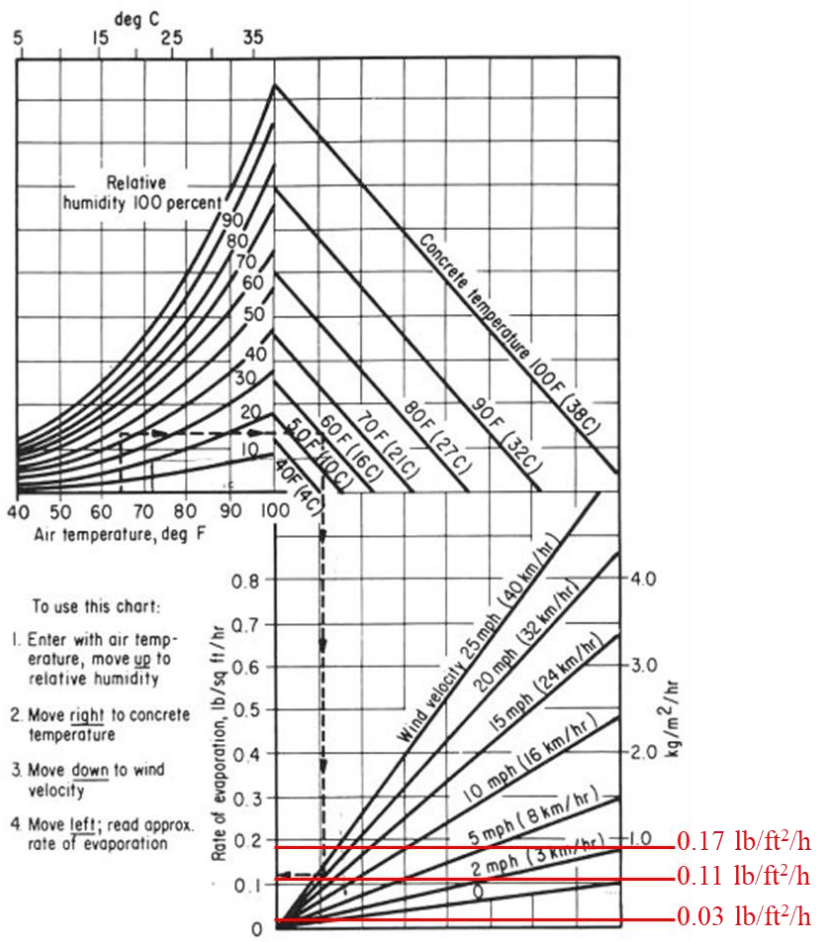

FIGURE 10 Nomograph for estimating surface water evaporation rate of concrete (10)

Testing Environment

The concrete samples were tested in three different environments, as summarized in TABLE 1. The 0.03 and 0.11 lb/ft^2/h evaporation rates were obtained by storing the samples at 50% RH 73^{o}F and 100^{o}F, respectively. The highest evaporation rate was obtained by storing the concrete 12 inches away from a 250-watt heating lamp. A hydrocarbon sensor showed that the air temperature was 110^{o}F with a 12% RH. When wet curing was applied, three layers of water-soaked burlap were placed on the surface, and then this was sealed with aluminum tape to prevent evaporation. Every day, the burlap was removed, soaked with water, and placed on top of the sample. The air-curing sample was open to the environment.

TABLE 1 Curing Methods Applied to The Concrete Samples in Different Environments

Environments	Maximum Evaporation Rate	Temperature & Humidity	Curing methods applied to concrete samples
Low Evaporation	0.03 lb/ft^2/h	73°F+50% RH	Air curing, Continuous wet curing, and Wet curing after exposure for 3h, 6h, and 9h, respectively
Middle Evaporation	0.11 lb/ft^2/h	100°F+50% RH	Air curing, Continuous wet curing, and Wet curing after exposure for 3h, 6h, and 9h respectively
High Evaporation	0.17 lb/ft^2/h	110°F+12% RH	Air curing; Continuous wet curing; Wet curing after exposure for 2h, 4h, 6h, 8h, and 10h respectively

Diffusion coefficient

The diffusion coefficient (D_{ic}) for different evaporation rates and curing times is shown in FIGURE11, and a Student t-test between continuous wet curing and the other curing methods is shown in TABLE 2. In the t-test results, if the calculated t value is greater than the theatrical t value (2.447 in this case), the groups are categorized as not similar; otherwise, the groups are categorized as similar.

In all cases, the continuously wet-cured sample performed the best, and the air-cured sample performed the worst. Also, as the evaporation rate became more severe, the D_{ic} increased. As the D_{ic} increases, this means the resistance to outside chemical penetration also decreases, and this decreases the durability of the concrete.

All the samples cured at the lowest evaporation rate (0.03 lb/ft^2/h) seem to have a similar diffusion coefficient. A Student t-test was used to show that there is no statistical difference in these measurements. The results are shown in TABLE 2. This means that the drying did not impact the measured diffusion coefficient. In the lower evaporation rates (0.3 lb/ft^2/h), all the curing periods have a similar D_{ic} except for the air-cured sample. It doesn't appear that the D_{ic} detects a difference in delaying the curing to be placed on the concrete until at least a 9-hour delay, and this shows agreement with the t-test results. The delay in curing in this low evaporation rate environment does not seem to impact the diffusion coefficient.

At the highest evaporation rate (0.17 lb/ft^2/h), the continuously wet-cured sample has a higher D_{ic} than the other drying environments. This could be caused by the higher temperature impacting the uniformity and quality of the hydration products. Also, when the wet curing is delayed, this causes the D_{ic} to increase almost linearly with time until 8h. The results also show that even delaying the application of the wet curing by 2h will cause an increase in the diffusion coefficient. The t-test results also show that all the delayed wet curing has a statically different mean from the sample that was continuously wet cured. This shows that even a 2h delay in placing the wet curing can impact the D_{ic} in a high evaporation environment (0.17 lb/ft^2/h).

Care should be taken in evaluating the D_{ic} of the air-cured samples to the others. The air-cured samples will have a lower amount of water in their pores from drying that was never replenished with applied water. When the tracer solution is added to these samples, it will be drawn in by a combination of diffusion and absorption. This will make the measured D_{ic} appear to be larger. This doesn't occur in the wet cured samples because the water added to the surface increases the DOS, and so the movement of the outside fluid into the concrete would only be caused by diffusion.

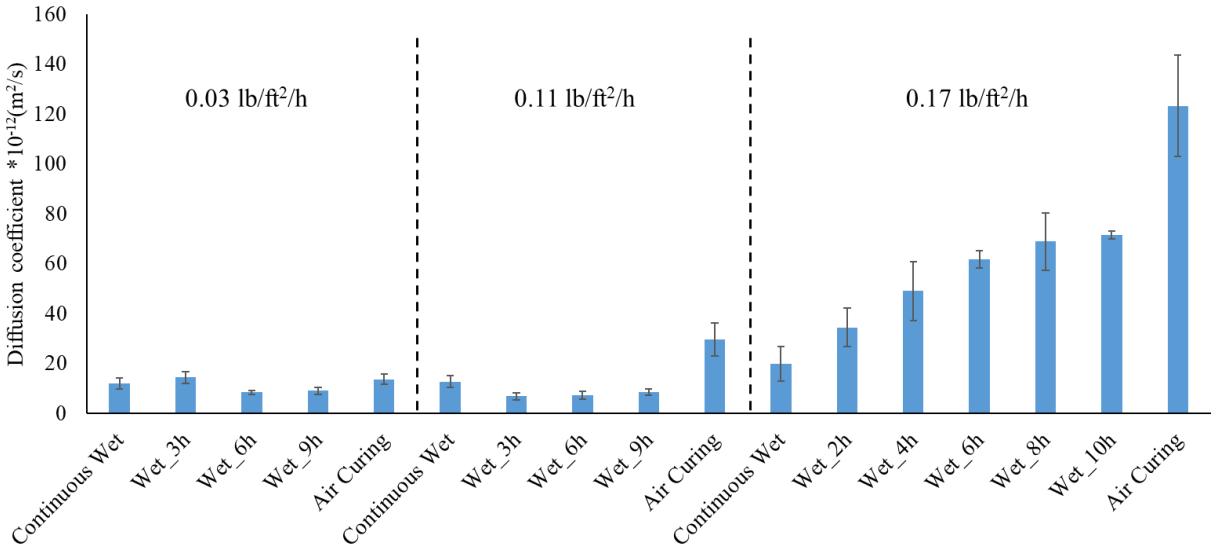

FIGURE11 Diffusion coefficient of the mortar samples under different curing methods

TABLE 2 Student t-test Result Between Continuous Wet Curing And the Other Curing Methods in Different Environments on the Diffusion Coefficient

Evaporation rate: 0.03 lb/ft^2/h						
	Wet_3h		Wet_6h	Wet_9h		Air Curing
Continuous Wet	1.46 similar		1.03 similar	0.75 similar		1.06 similar
Evaporation rate: 0.11 lb/ft^2/h						
	Wet_3h		Wet_6h	Wet_9h		Air Curing
Continuous Wet	2.35 similar		2.4 similar	1.66 similar		4.87 Not similar
Evaporation rate: 0.17 lb/ft^2/h						
	Wet_2h	Wet_4h	Wet_6h	Wet_8h	Wet_10h	AirCuring
Continuous Wet	2.87 Not similar	4.27 Not similar	10.93 Not similar	7.34 Not similar	14.55 Not similar	9.63 Not similar

1. The t-test hypothesis is that the two-group means are the same.
2. Parameters for the t-test:
significance value $\alpha = 0.05$; degree of freedom = 6; theoretical t value = 2.447.

Practical Significance

This work shows that the CHIP can quantify how wet curing impacts the quality of the resulting concrete. This is important information to quantify because the diffusion coefficients are an indicator of the long-term durability of the concrete, and this can be quantified by the CHIP. This highlights how the CHIP could be used in the field after the concrete is in place to determine the quality of the material, construction, and curing. This highlights how the CHIP could be used as an in place specification for concrete and ensure the SHAs are receiving concrete with the necessary durability. More details about this work are available in other publications (11).

The ability of silane to reduce ion penetration

To prevent the penetration of outside fluids into concrete, one strategy is to use surface treatments that are applied on the exposed surface of the concrete. This case study will study the effectiveness of silanes. Silanes are categorized as vapor-permeable sealers. Previous research shows that the application of silanes on the concrete surface significantly reduces the ingress of outside chemicals, thus reducing the chloride ions penetrations and reducing the corrosion of steel reinforcement. The Oklahoma Department of Transportation (ODOT) specifies the use of silane coatings on all bridge decks with a minimum thickness of 1/8 inch. This work investigates the performance of 14 cores from ODOT bridge decks to investigate the performance of the silane and the underlying concrete with the CHIP.

Depth of Penetration of Outside Chemicals

From each of the 14 samples, 4 smaller cores of ¾ inch diameter were extracted: 2 cores from the top with the silane and 2 cores from the side without silane. An overview is shown in **Error! Reference source not found.** These cores were also inspected to make sure that they did not contain a large aggregate near their surface, as this would interfere with the diffusion measurement. If this occurred, then another core was taken. Next, the cores were oven-dried at 50°C until a state of mass equilibrium was reached, at which less than 0.03% weight change occurred in 24 hours. That mass equilibrium was reached in 5 days. After this, the Degree of Saturation (DoS) of the cores was recorded, which was 2.05±0.48 %. Then, the sides of the cores, except the surface, were coated with hydrophobic wax to force the outside fluid to penetrate in only one direction from the unwaxed top, as shown in FIGURE 12(b).

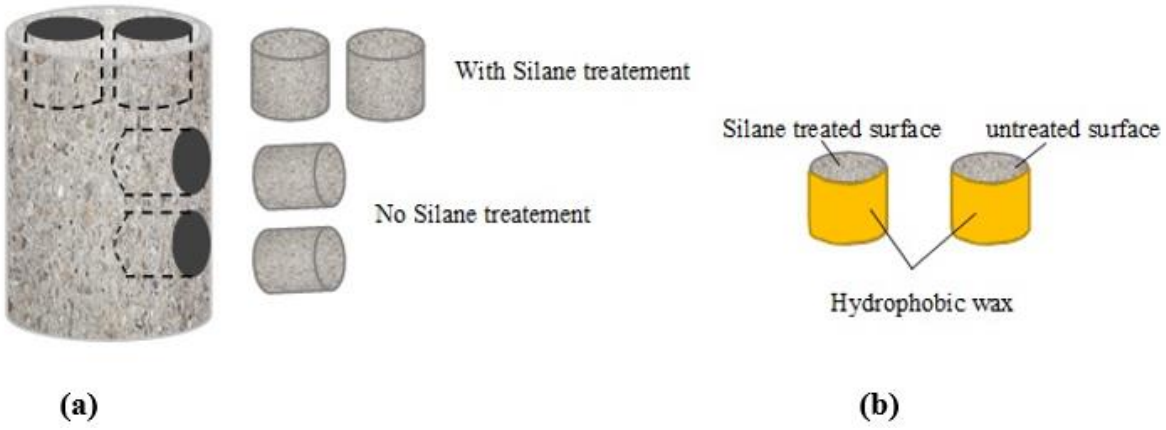

FIGURE 12 illustrates (a) the extraction of ¾-inch diameter cores from each sample and (b) the application of wax on the sides and bottom of each core.

Performance of silane coating

An iodide concentration profile for a sample is shown in FIGURE 13. The dashed line represents the data of the smaller cores taken from the side without any silane treatment, and the solid lines show the data for the silane-treated smaller cores taken from the top of the sample. Each silane (solid line) and non-silane (dashed line) is an average of four concentration profiles; two smaller cores are imaged from two directions, resulting in a total of four profiles for silane cores and a similar manner, four profiles for non-silane cores.

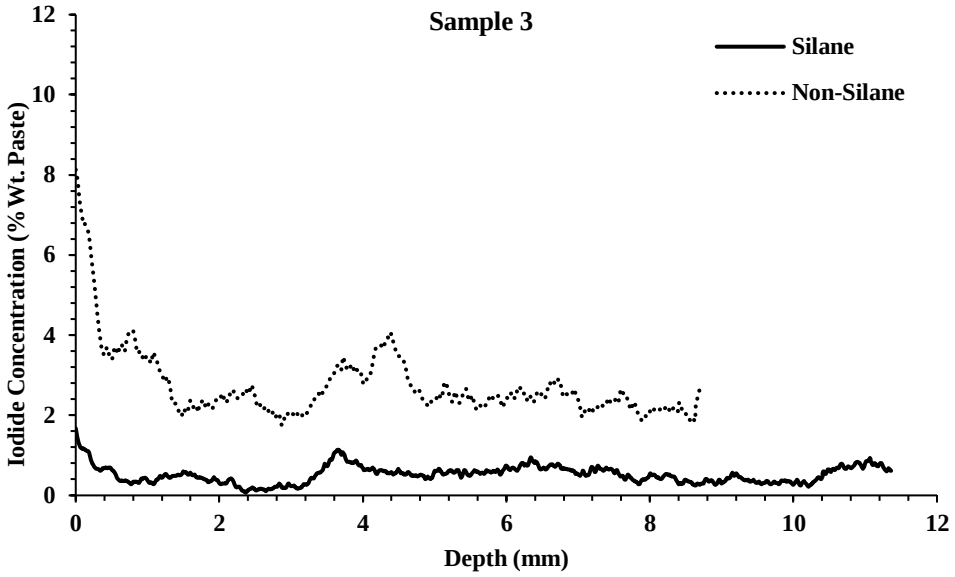

FIGURE 13 The iodide concentration profile of sample 3

The iodide concentration profiles of all silane-treated samples collected from 14 locations are shown in FIGURE 14. It can be observed that the application of silane decreases the iodide concentration and is effective in keeping the outside chemicals from penetrating. However, in some cases, the concentration values at greater depths for silane and non-silane samples came very close. In some of the samples, such as sample 2, it can be observed that the concentration values are low for silane samples near the surface, but as the depth increases, the concentration profiles increase and get closer to non-silane samples.

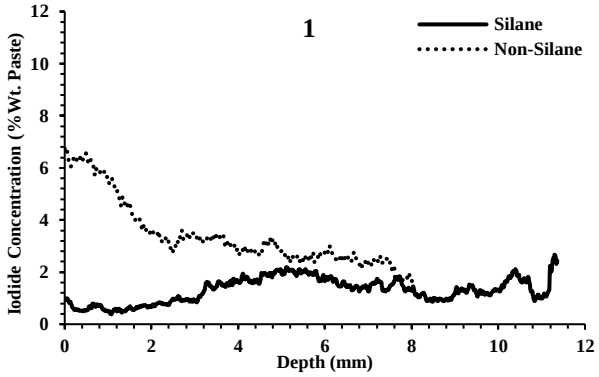
1
Silane
Non-Silane
Iodide Concentration (% Wt. Paste)
Depth (mm)
0
2
4
6
8
10
12

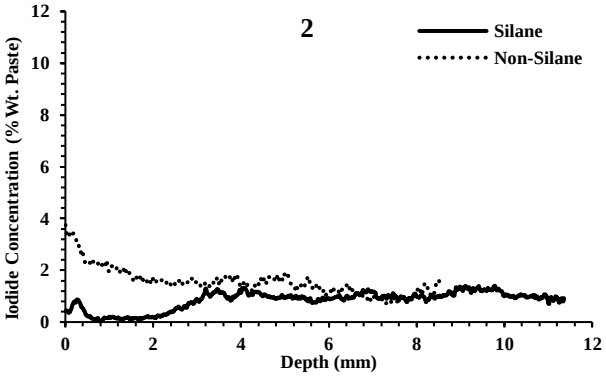
2
Silane
Non-Silane
Iodide Concentration (% Wt. Paste)
Depth (mm)
0
2
4
6
8
10
12

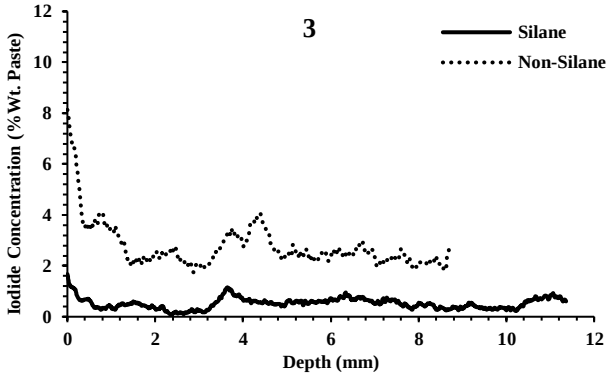
3
Silane
Non-Silane
Iodide Concentration (% Wt. Paste)
Depth (mm)
0
2
4
6
8
10
12

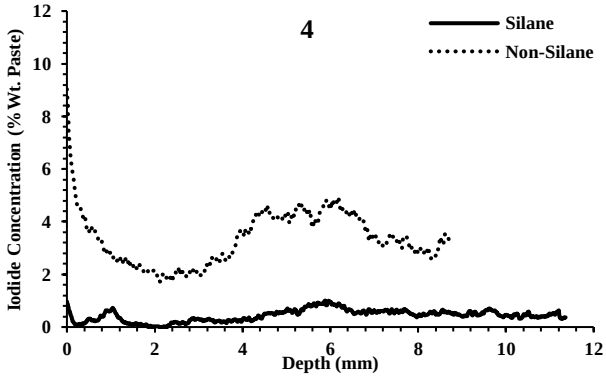
4
Silane
Non-Silane
Iodide Concentration (% Wt. Paste)
Depth (mm)
0
2
4
6
8
10
12

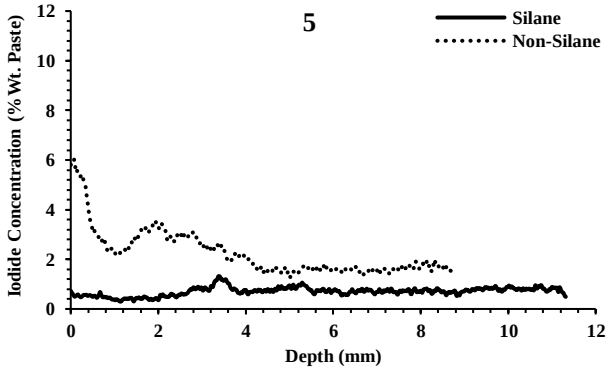
5
Silane
Non-Silane
Iodide Concentration (% Wt. Paste)
Depth (mm)
0
2
4
6
8
10
12

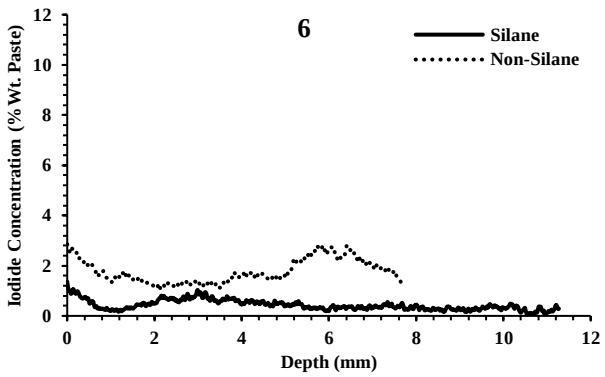
6
Silane
Non-Silane
Iodide Concentration (% Wt. Paste)
Depth (mm)
0
2
4
6
8
10
12

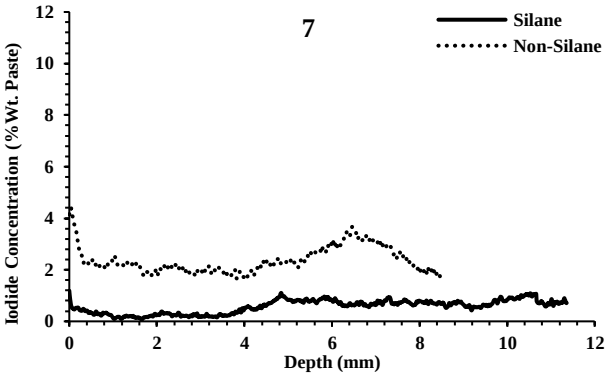
7
Silane
Non-Silane
Iodide Concentration (% Wt. Paste)
Depth (mm)
0
2
4
6
8
10
12

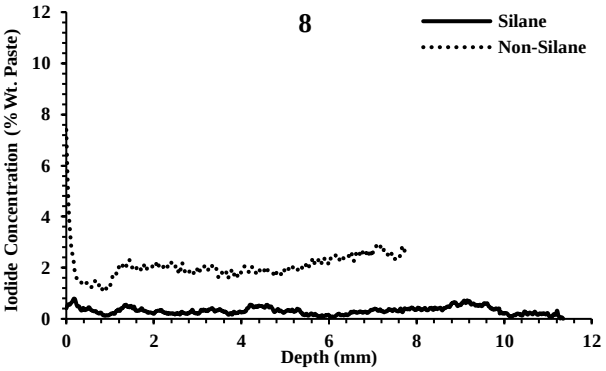
8
Silane
Non-Silane
Iodide Concentration (% Wt. Paste)
Depth (mm)
0
2
4
6
8
10
12

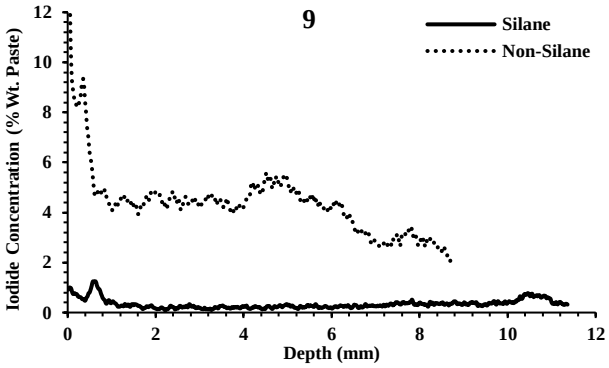
9
Silane
Non-Silane
Iodide Concentration (% Wt. Paste)
Depth (mm)
0
2
4
6
8
10
12

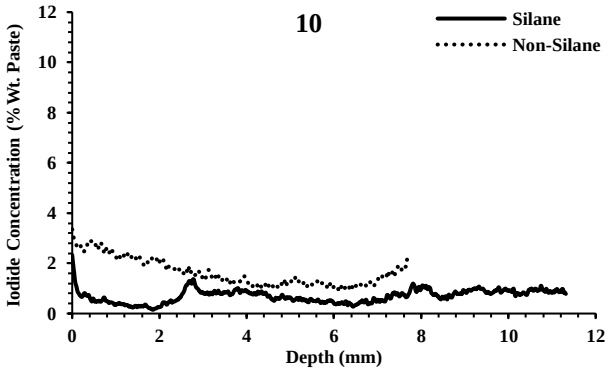
10
Silane
Non-Silane
Iodide Concentration (% Wt. Paste)
Depth (mm)
0
2
4
6
8
10
12

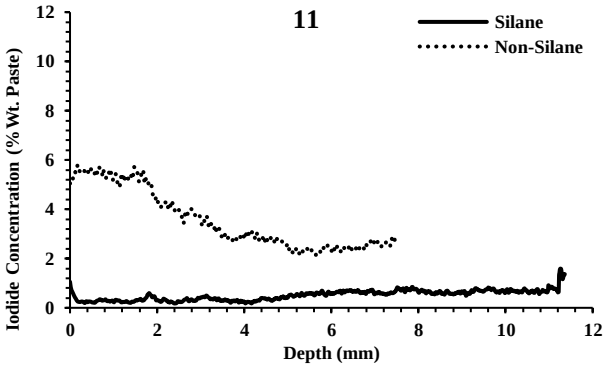
11
Silane
Non-Silane
Iodide Concentration (% Wt. Paste)
Depth (mm)
0
2
4
6
8
10
12

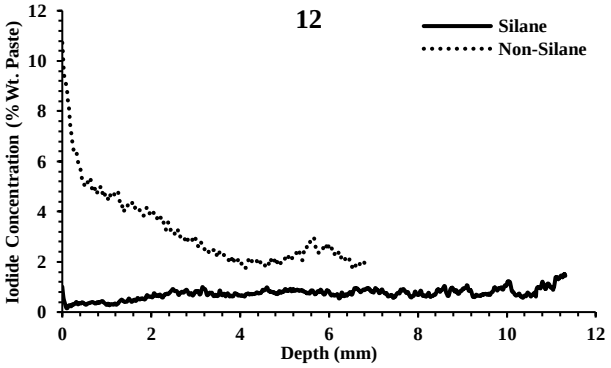
12
Silane
Non-Silane
Iodide Concentration (% Wt. Paste)
Depth (mm)
0
2
4
6
8
10
12

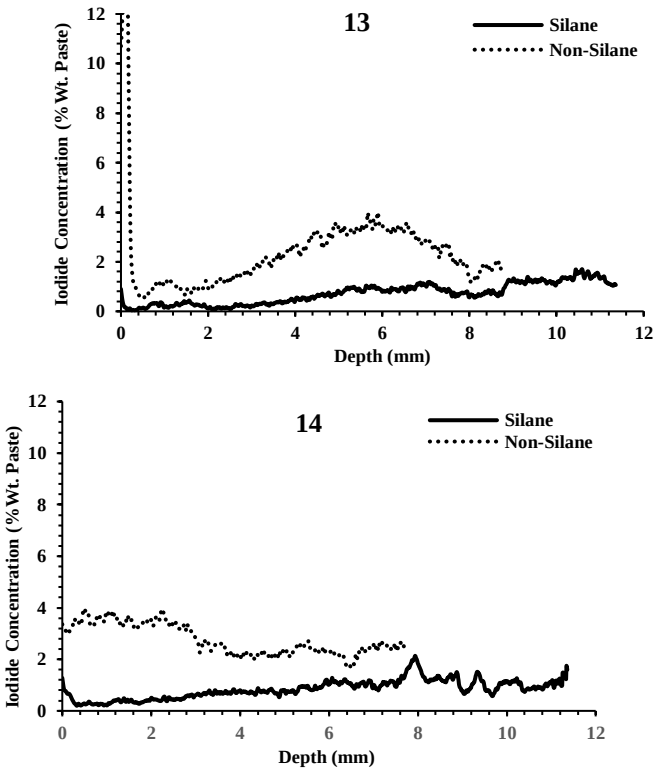

FIGURE 14 The iodide concentration profiles of all silane-treated samples collected from 14 locations

FIGURE 15 compares the iodide concentrations of all the samples at a fixed depth of 2 mm for both the silane and non-silane samples. A depth of 2 mm was chosen as it avoided any surface effects and provided insights into the concentration of the tracer at the surface.

The concentrations in non-silane samples are much higher than in silane samples, which suggests that the silane coating is effective in reducing the penetration of outside chemicals. The average concentration from all non-silane samples at a depth of 2 mm is 2.7%, while the average value for silane-treated samples at the same depth is 0.3%. This shows that the silane application reduces the penetration of outside chemicals by 8.5 times compared to samples without silane.

For the non-silane samples, there exists a large variability among the samples. Some samples have iodide concentrations as low as 1% by weight, and some have greater than 4%. This may be caused by the variation in the mixture design and the curing methods employed for these samples.

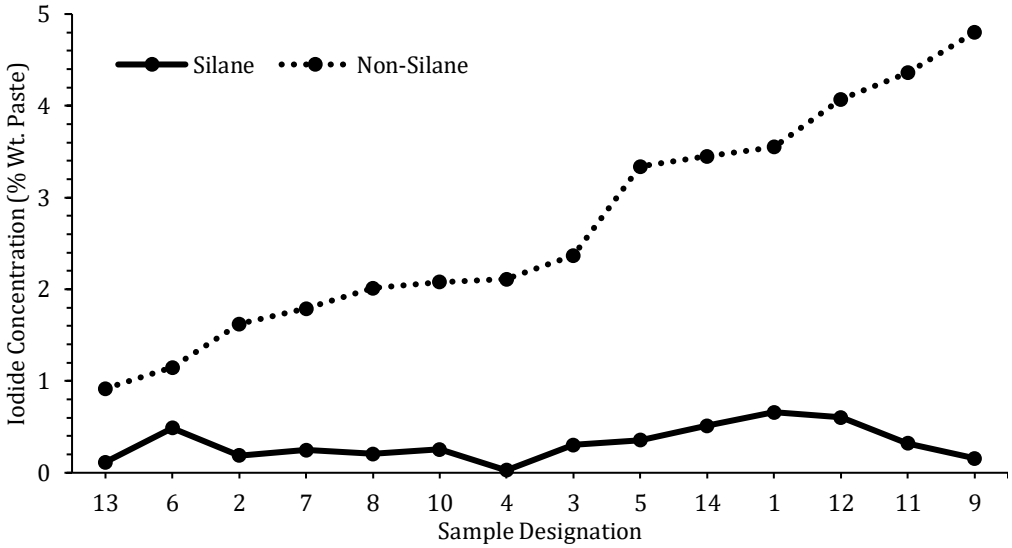

FIGURE 15 A comparison of silane vs. non-silane samples at 2mm depth

Practical Significance

This shows that the CHIP can be used to investigate the effectiveness of surface coatings on concrete. This could be used to determine if a surface coating is still effective or if that coating has been applied correctly. This again shows the usefulness of the CHIP. More information about this testing can be found in other publications (12).

Impact of fly ash on diffusion

It is widely known that fly ash is a useful tool to reduce the diffusion coefficient of a concrete mixture over time; however, there is little information about how different fly ashes perform. Also, most testing in concrete is done between 28 and 56 days. This work shows that fly ash continues to react over time and that the performance at 56 days may not be indicative of the long-term performance at 700 days.

FIGURE 16 shows the measured D_{ic} of mixtures with 20% fly ash replacement. The data on the far right is from a sample with only ordinary Portland cement (OPC). FIGURE 16 shows the changes in the D_{ic} over time are very different for OPC compared to mixtures that contain fly ash. For example, the OPC D_{ic} decreases almost linearly with time, and the fly ash sample decreases more rapidly over the first 200 d and then stays almost constant or decreases slowly. These differences in the change of the D_{ic} with time are probably attributed to the differences in the hydration reactions between the two systems.

The concrete industry currently prefers Class F fly ashes because they are supposed to provide a better improvement in concrete durability; however, this work shows that many Class C fly ashes provide comparable diffusion coefficients to Class F fly ash after 500 to 700 days of curing. This can be very helpful.

Other work is ongoing to use the bulk oxide content to determine which Class C fly ash performs similarly to Class F fly ash. This will be published in future work.

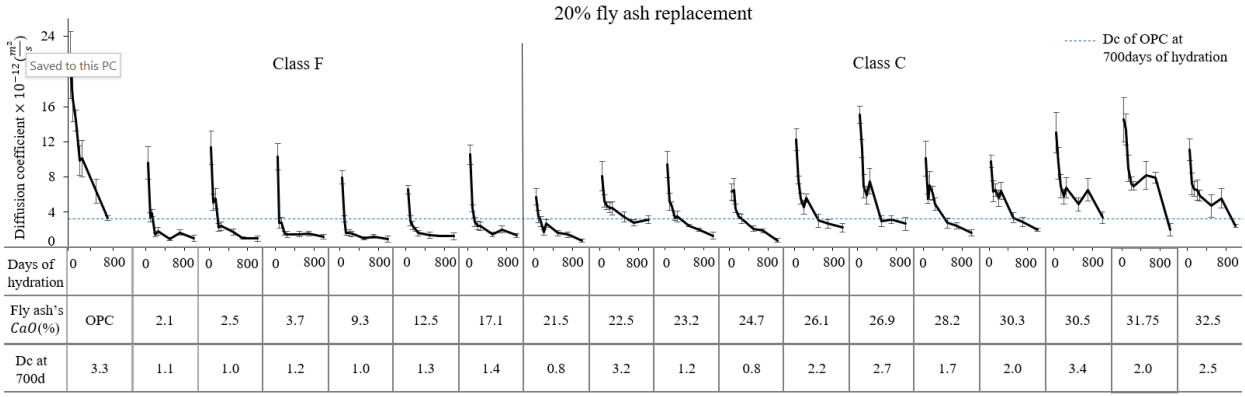

Days of hydration	0 800	0 800	0 800	0 800	0 800	0 800	0 800	0 800	0 800	0 800	0 800	0 800	0 800	0 800	0 800	0 800	0 800	0 800	0 800
Fly ash's CaO(%)	OPC	2.1	2.5	3.7	9.3	12.5	17.1	21.5	22.5	23.2	24.7	26.1	26.9	28.2	30.3	30.5	31.75	32.5	
Dc at 700d	3.3	1.1	1.0	1.2	1.0	1.3	1.4	0.8	3.2	1.2	0.8	2.2	2.7	1.7	2.0	3.4	2.0	2.5	

FIGURE 16 The diffusion coefficient as measured by the Chip for 17 different fly ashes used at 20% replacement level and OPC.

Practical Significance

The CHIP can provide rapid feedback on different mixture proportions and show the potential improvements that can be applied to concrete mixtures. This also shows that measurements within the first 90 days do not provide insight into the long-term performance of the concrete mixtures. This shows that there is more to understand about Class C fly ash and its long-term performance.

Stage 1 Report

The Stage 1 report was submitted on 8/1/22. A meeting was held with the research oversight committee to review the work, and it was approved for Stage 2.

The goal of this task is to evaluate the repeatability of the CHIP to measure concrete and paste samples. This work also determined the minimum number of angles needed to investigate a sample and determine an accurate estimate of the diffusion coefficient. Using the minimum number of angles will save the user time while still providing an accurate measurement.

Evaluating the impact of different strip wishts on concentration profiles

Sample preparation

A total of 27 mixes for paste and concrete were examined (104 samples for paste and 104 samples for concrete). These mixtures used different fly ash types and replacement levels as well as at different ages.

The paste samples were cast using cylindrical molds with a 9.5 mm diameter and 46 mm depth. Samples were sealed and cured at 23°C in a temperature-controlled room with no additional water added. Half of the paste samples investigated were 1000 days old, and the other half were 45 days old.

The concrete samples investigated in the CHIP were drilled from larger concrete cylinders. The cores were 19mm (3/4 in) diameter and approximately 35 mm deep. Four cores were taken from each cylinder. Half of the concrete samples were 1100 days old at coring, and the other half were 45 days old. The 45-day-old samples were cured in a moist room at 23°C, following the specifications outlined in ASTM C511. The 1100-day-old samples were cured inside of plastic molds in a temperature control room.

Before starting the test, the concrete samples were vacuum saturated for two hours with a vacuum of 37mmHg ± 5mmHg, followed by a resting period of 24 hours in a sealed bag at atmospheric pressure and 23^{o}C. This was done to fill the pores by vacuum saturating the sample and then giving the larger pores time to empty. This is done to give the samples a consistent condition before they are tested and to represent a saturated condition that may occur in the field.

Wax was applied to all surfaces of the samples except for the finished surface. These samples were then placed in a salt solution, and the wax ensured that all diffusion was from the top surface. This created a one-dimensional diffusion into the sample.

Data analysis for cores

Previous studies used a constant width of 0.9 mm at the center of the sample to minimize the impact of beam hardening. If the sample is largely homogeneous, such as paste and mortar, then this approach may be sufficient. However, to reduce the variability for a concrete mixture, a wider strip may be helpful. This study compared using 0.9 mm, 8 mm, and 18 mm strips for paste and concrete samples. It should be noted that considering the exact whole width of a sample is not possible as edge chipping can occur during demolding or coring, which can impact the results. FIGURE 17 shows a schematic view of narrow and wide strips for paste and concrete samples. FIGURE 18 shows the differences in measured gray values for the different widths. It shows that the average gray value increases with the inclusion of a wider strip. Because of the curvature of the sample, the larger width penetrates less material, and this leads to lower X-ray absorption when measuring a sample.

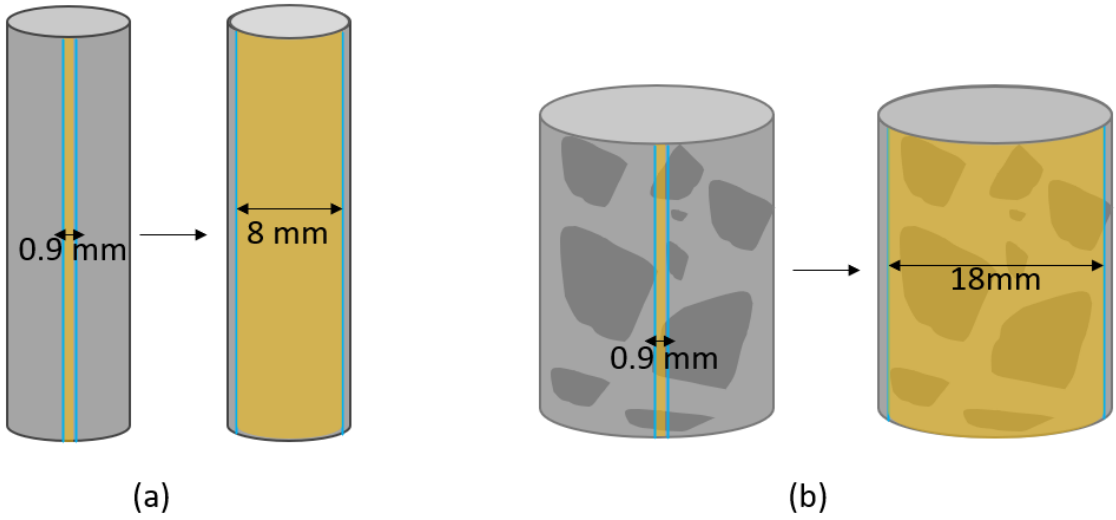

FIGURE 17 A schematic view of different strip widths: a) paste sample, b) concrete sample.

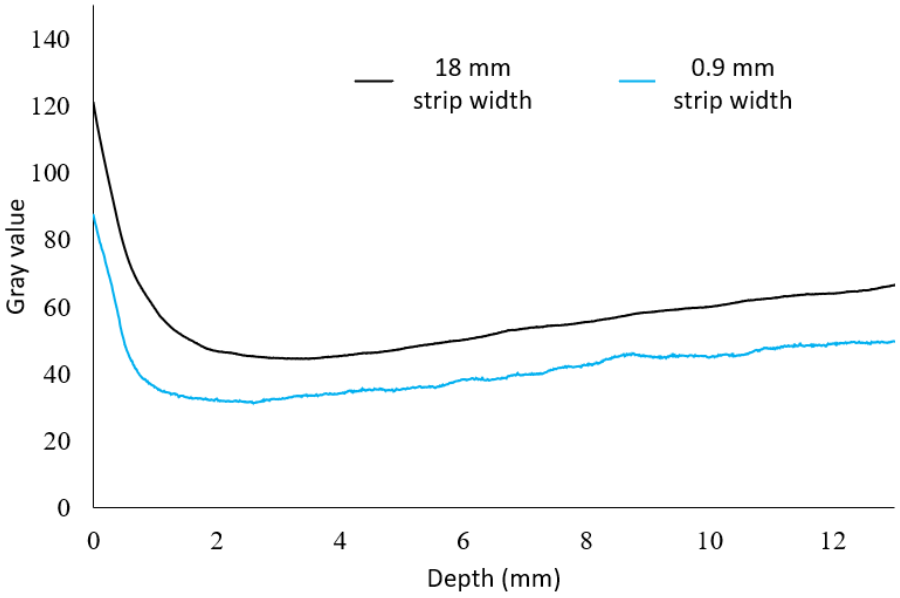

FIGURE 18 Gray value vs. depth for 0.88mm and 18 mm strip width

To address this issue, a thickness correction factor is introduced. This factor is defined in Equation 1:

$$\text{Thickness correction factor} = \frac{\text{Avg gray value of the center pixel}}{\text{Avg gray value on width n}} \quad 0 < n < x \qquad (1)$$

The term 'Avg gray value of the center' refers to the average gray value over height observed at the center of the sample. On the other hand, the 'Avg gray value on width n' represents the average gray value over height observed at any location across the width of the sample. The width 'x' for concrete samples ranges from 0 to 18 mm, while for paste samples, it ranges from 0 to 8 mm.

After finding the thickness correction factor this is multiplied by the average gray value of each width. This will eliminate the influence of the sample's thickness in the gray value measurements. FIGURE 19 provides a visual representation of the average gray value across the width at the center of the sample. FIGURE 19a separates seven strips over the width of the samples; each is 1.5mm wide, highlighted for visual reference. The average gray in each strip is presented in FIGURE 19b.

Notably, the gray values of the strips near the edges appear higher due to increased brightness in the image caused by the reduced thickness of the sample near the edges.

FIGURE 19c shows the same values as FIGURE 19b after applying the geometric correction factor. After this correction, the average gray value of each highlighted area becomes equal. This finding indicates that the sample's thickness no longer affects the gray values, demonstrating the effectiveness of the geometric correction. All wider images use the geometric correction.

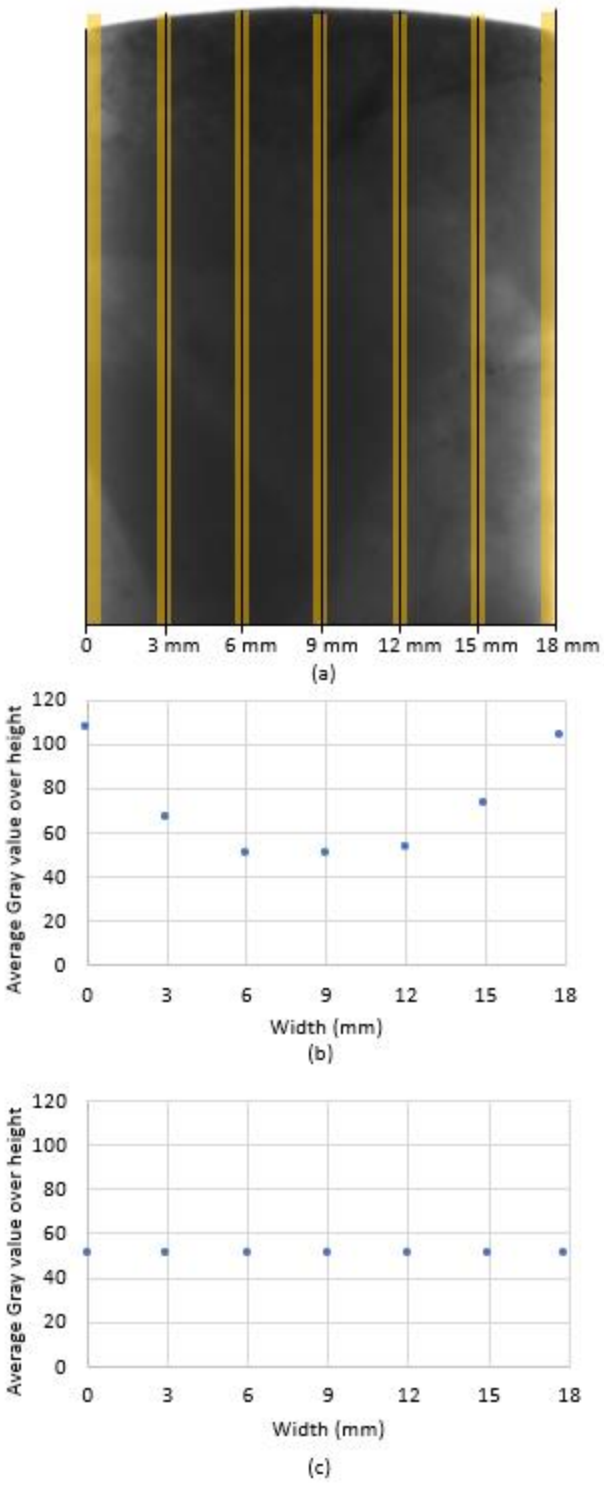

FIGURE 19 a) a concrete sample that shows seven highlighted strips, b) before the correction factor, and c) after applying the correction factor.

Paste

The concentration profile of a typical paste sample, radiographed from two angles, is presented in FIGURE 20. FIGURE 20a shows the concentration profile based on a 0.9 mm strip, and FIGURE 20b shows the concentration profile for an 8 mm strip width. Both results are similar.

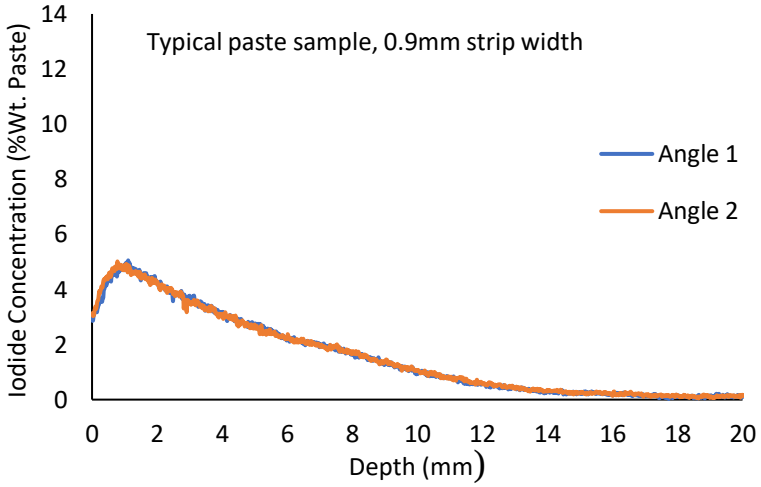

(a)

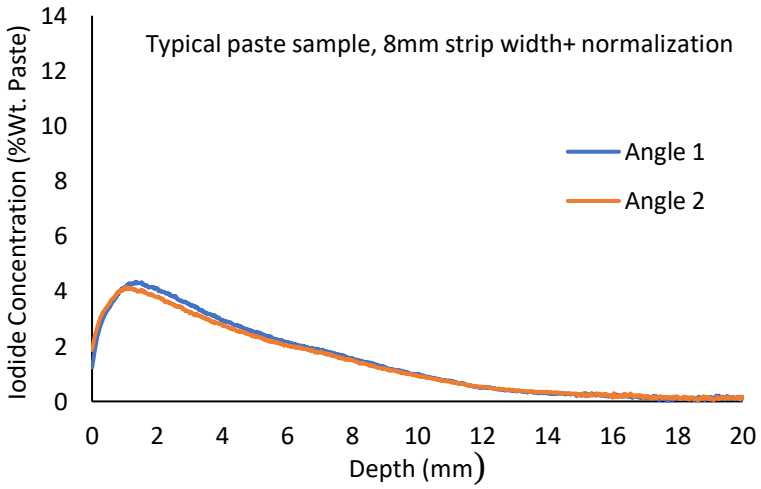

(b)

FIGURE 20 The concentration profile for a typical paste sample is radiographed from 2 sides; a) data analysis is performed on a 0.9 mm strip width, and b) data analysis is performed on an 8 mm strip width.

FIGURE 21, a, and b show the results for all 104 paste samples, including 20% and 40% fly ash replacements. Based on FIGURE 21, the results obtained from both analysis approaches seem identical. TABLE 3 compares the D_{ic} by showing the average, standard deviation, coefficient of variation, and average R square for two angles of each sample. The findings reveal that considering a larger width (8 mm)

and applying the geometric correction factor leads to a 0.5% decrease in the coefficient of variation and a 0.24% increase in the R square for paste samples. These changes are negligible, and it shows that the average coefficient of variation for a paste sample is approximately 20%. These findings show that the larger strip and geometric correction factor exhibit values similar to those of the smaller analyzing area, confirming the accurate application of geometric correction factors. Additionally, it underscores the redundancy of analyzing a larger area with paste samples.

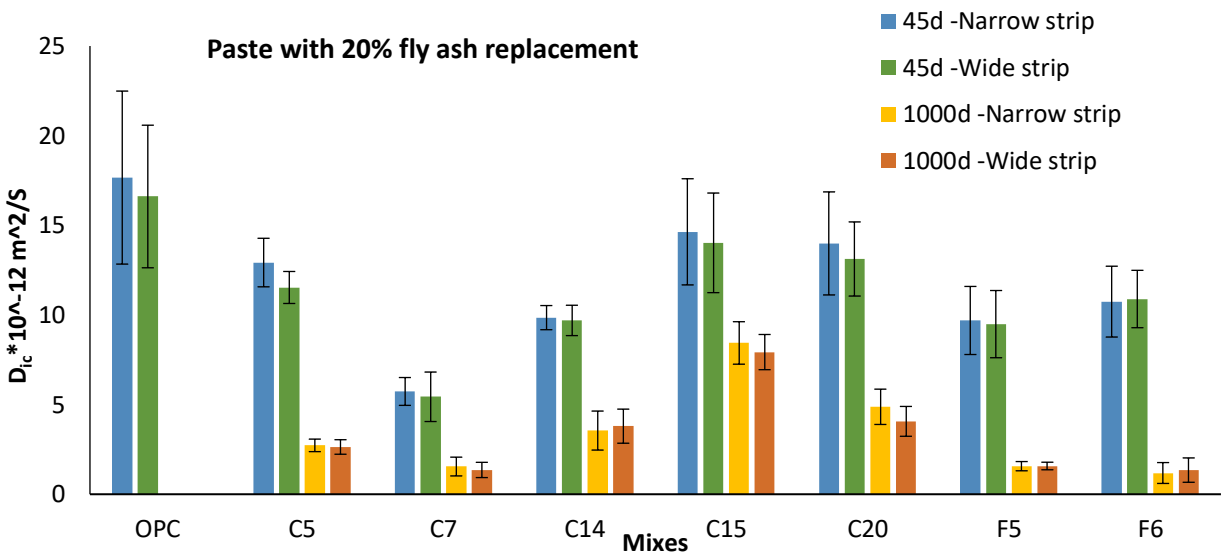

(a)

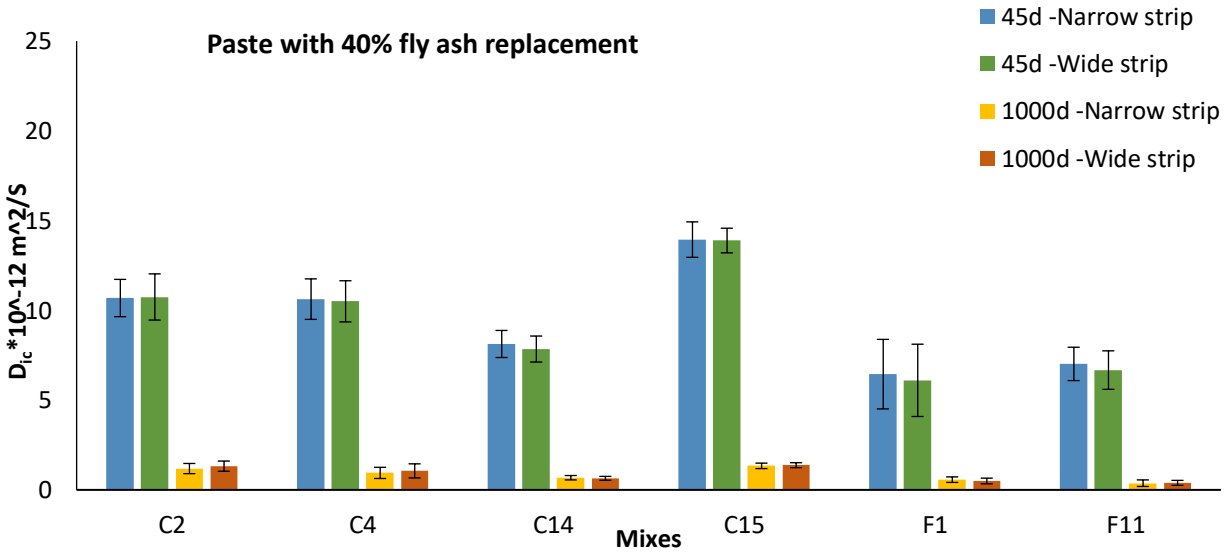

(b)

FIGURE 21 A comparison between two methods of image analysis for paste samples: 1) considering the 0.9mm strip at the center of the sample, 2) considering the 8mm strip width of the sample. a) Paste samples with 20% fly ash replacement paste samples. b) Paste samples

TABLE 3 A Comparison Between The Coefficient of Variation and R Square of Two Methods of Image Analysis for Paste Samples: 1) Considering the 0.9mm Strip at The Center of The Sample, 2) Considering The 8mm Strip Width of The Sample.

			Coefficient of variation		R square	
Fly ash type	Fly ash replacement	Age	0.9mm	8mm	0.9mm	8mm
OPC	20%	45	27.32%	23.95%	96.45%	99.45%
		1000	-	-	-	-
C5	20%	45	10.48%	7.74%	99.23%	99.48%
		1000	12.87%	15.37%	95.13%	95.40%
C7	20%	45	13.54%	25.40%	99.10%	99.40%
		1000	33.95%	31.41%	98.25%	99.37%
C14	20%	45	6.84%	8.74%	98.11%	99.35%
		1000	30.62%	25.05%	97.54%	97.84%
C15	20%	45	20.24%	19.81%	99.21%	99.45%
		1000	14.03%	12.39%	97.52%	97.76%
C20	20%	45	20.54%	15.74%	96.25%	98.25%
		1000	20.21%	20.48%	97.25%	98.54%
F5	20%	45	19.59%	19.76%	99.67%	99.82%
		1100	16.49%	13.42%	96.83%	96.81%
F6	20%	45	18.37%	14.70%	99.55%	99.72%
		1000	49.16%	50.43%	95.72%	93.85%
C2	40%	45	9.72%	11.96%	99.00%	99.22%
		1000	23.87%	21.47%	97.62%	97.88%
C4	40%	45	10.61%	10.92%	99.08%	99.48%
		1000	33.00%	37.05%	96.73%	97.18%
C14	40%	45	9.27%	9.22%	98.17%	98.64%
		1000	18.25%	16.53%	95.02%	84.10%
C15	40%	45	7.07%	4.94%	97.97%	98.35%
		1000	11.50%	10.04%	93.73%	95.77%
F1	40%	45	30.05%	32.99%	98.07%	97.39%
		1000	26.83%	32.02%	98.27%	99.55%
F11	40%	45	13.24%	16.05%	99.46%	99.54%
		1000	48.86%	35.38%	91.85%	95.66%
Average			20.61%	20.11%	97.44%	97.68%

This study uses ANOVA mixed-effects models with repeated measures to statistically assess the variations in D_{ic} between the two widths. The D_{ic} is the continuous outcome variable in this model. Fly ash type, replacement level, and sample age are fixed effects, while the two widths are allowed to vary. The repeated measure model is applied to the data as the same image is analyzed using both test methods.

The ANOVA mixed-effect model utilizes the p-value, or probability value, to quantify the likelihood of the observed data occurring under the null hypothesis calculated by the test statistic's probability. The null hypothesis assumes there is a significant difference in the analysis results between using a narrow and wide strip with applying a geometric correction factor, regardless of fixed effects. A p-value higher than 0.05 shows the null hypothesis is true or there is no statistical difference between the variables.

TABLE 4 presents the outcomes of the ANOVA analysis for the paste samples. The results indicate that the fly ash type, level of replacement, and age of the samples provide statistically significant differences, as their respective p-values exceed 0.05. Importantly, TABLE 4 demonstrates there are no significant differences between analyzing images using narrow and wide strips, as indicated by the almost zero p-values.

TABLE 4 ANOVA Model For The Impact of Different Variables on The Analysis

Factors	P-value	Significance
Fly ash type	0.895	Statistically Significant
Fly ash replacement	1.265	Statistically Significant
Age	0.476	Statistically Significant
Width of analysis	0.000	Not Statistically Significant

In conclusion, the findings from FIGURE 21**,** TABLE 3**,** and TABLE 4 collectively support that considering a wider strip by applying a geometric correction factor does not change the value or accuracy of the measured diffusion coefficient.

Concrete

FIGURE 22 shows a typical concentration profile for a concrete sample radiographed from 3 angles with two different strip widths. FIGURE 22a shows a data analysis considering a 0.9mm strip width, and FIGURE 22b shows the same angles when an 18 mm strip is used. The profile for the smaller strip has higher noise as the curves are not as smooth. This shows that the measurement is impacted by local inhomogeneous regions caused by aggregates when a 0.9 mm strip is used. The 19 mm data shows that the measurements show similar results after approximately 4mm in depth from the surface. This has the potential to improve the accuracy of the measurement.

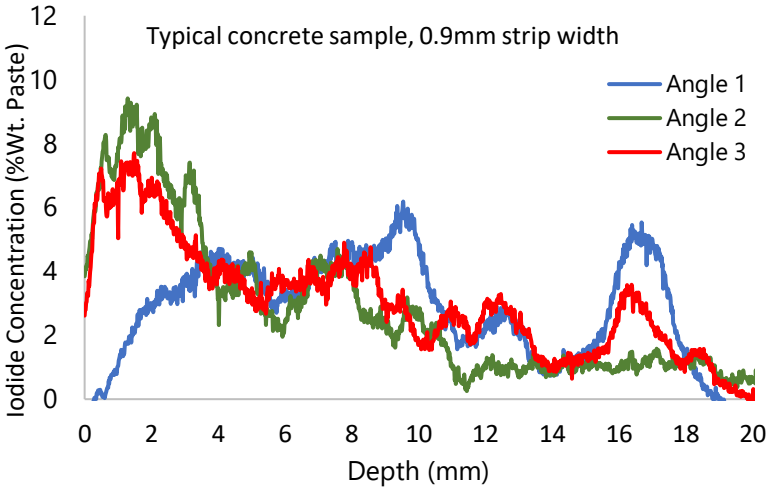

(a)

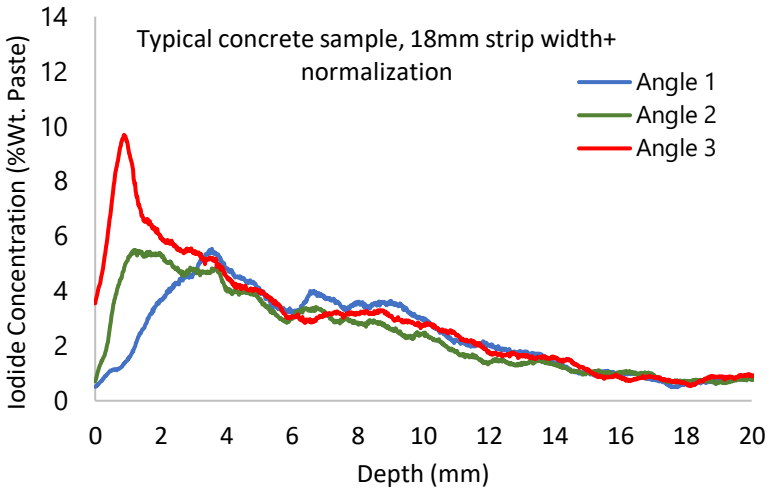

(b)

FIGURE 22 The concentration profile for a typical concrete sample is radiographed from 3 sides: a) data analysis is performed on a 0.9 mm strip width, b) data analysis is performed on an 18 mm strip width plus applying a geometric correction factor.

In order to improve the results, the sample is investigated from nine different angles with approximately a 40° angle between each radiograph. FIGURE 23**Error! Reference source not found.** shows the different angles used to analyze the sample. Using a greater number of angles allows more angles to be used to minimize the impact of the large aggregates on the results.

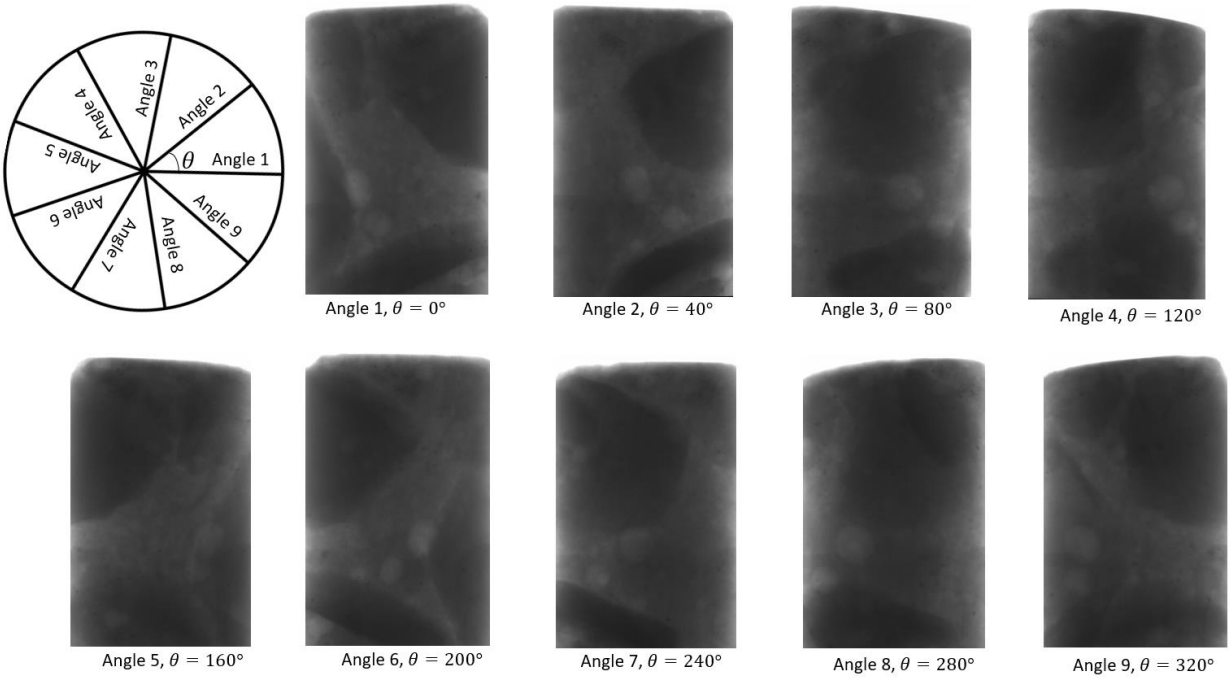

FIGURE 23 Taking images from 9 different angles.

FIGURE 24 A comparison between two methods of image analysis for concrete samples: 1) considering a 0.9 mm strip at the center of the sample and 2) considering an 18 mm width. Figure**Error! Reference source not found.** a and b represent the D_{ic} obtained from using 9 different angles with different strip widths. When a 0.9 mm strip was used, the standard deviations were routinely higher than when an 18 mm strip was used. The means are also different for several of the samples. This suggests that a narrow strip width does not investigate enough sample volume for the concrete samples presented.

TABLE 5 shows the changes in the coefficient of variation and R square values from different analysis widths. By using the larger width, the average coefficient of variation decreases from 74.33% to 27.31%. This shows a significant decrease in the variance of the results. Additionally, TABLE 5 demonstrates that the average R square value, representing the fit of the non-linear regression model on concentration data, increases from 77.62% to 91.77%. These results highlight the improvement that a wider width makes in the estimate of the D_{ic}.

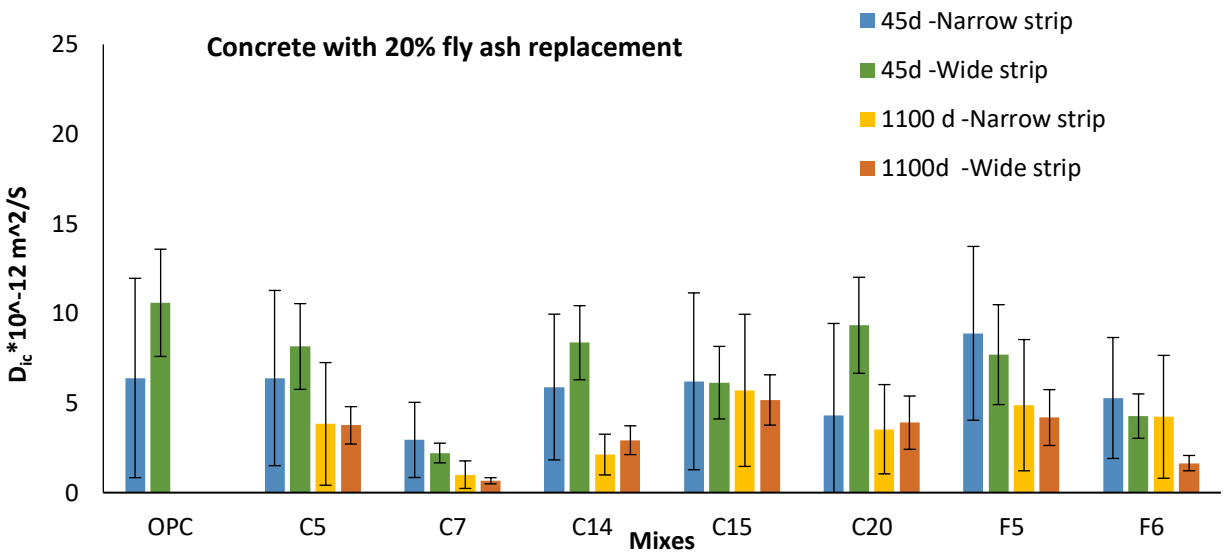

(a)

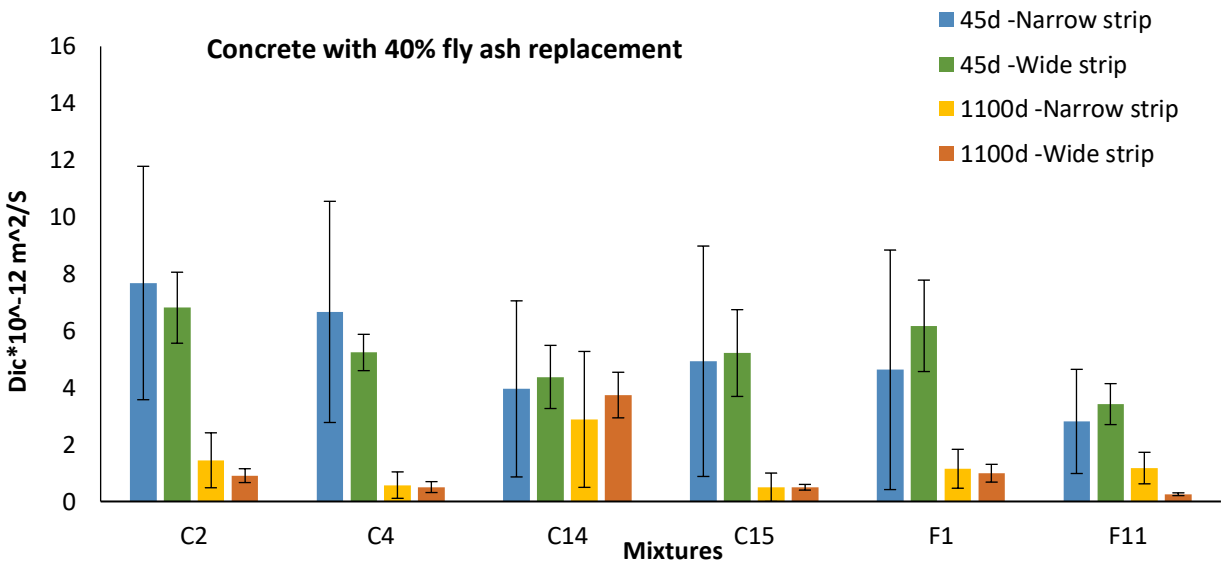

(b)

FIGURE 24 A comparison between two methods of image analysis for concrete samples: 1) considering a 0.9 mm strip at the center of the sample and 2) considering an 18 mm width. Figure a) Concrete samples with 20% fly ash replacement paste samples b) Concrete sample

TABLE 5 A Comparison Between The Coefficient of Variation And R Square of Two Methods of Image Analysis For Concrete Samples: 1) Considering a 0.9 mm Width at The Center of The Sample, 2) Considering an 18 mm Width of The Sample.

			Coefficient of variation		R square	
Fly ash type	Fly ash replacement	Age (days)	Narrow	Wide	Narrow	Wide
OPC	20%	45	86.98%	28.26%	70.46%	94.19%
		1100	-	-	-	-
C5	20%	45	76.44%	29.34%	74.44%	89.99%
		1100	89.19%	27.74%	77.20%	80.83%
C7	20%	45	71.31%	24.96%	86.78%	96.28%
		1100	76.44%	26.03%	46.86%	87.00%
C14	20%	45	69.04%	24.72%	80.97%	87.00%
		1100	53.61%	27.45%	87.40%	94.96%
C15	20%	45	79.42%	33.01%	75.00%	97.10%
		1100	74.34%	27.16%	68.52%	92.81%
C20	20%	45	119.95%	28.69%	81.66%	93.44%
		1100	70.40%	38.05%	86.66%	98.73%
F5	20%	45	54.58%	36.19%	73.61%	95.17%
		1100	75.03%	37.21%	72.55%	85.16%
F6	20%	45	63.88%	28.97%	72.15%	92.46%
		1100	81.03%	26.00%	78.43%	89.93%
C2	40%	45	53.42%	18.32%	75.67%	86.84%
		1100	66.72%	26.83%	65.43%	86.18%
C4	40%	45	58.34%	12.19%	81.91%	94.54%
		1100	80.75%	37.91%	85.00%	97.42%
C14	40%	45	78.23%	25.35%	86.96%	97.09%
		1100	82.81%	21.44%	82.21%	83.51%
C15	40%	45	82.17%	29.24%	69.99%	89.61%
		1100	100.00%	20.00%	72.69%	91.85%
F1	40%	45	90.98%	26.03%	76.33%	90.73%
		1100	59.48%	31.39%	84.63%	96.52%
F11	40%	45	65.05%	21.04%	91.45%	96.12%
		1100	47.21%	19.02%	90.89%	92.26%
Average			74.33%	27.13%	77.62%	91.77%

Number of angles

As previously mentioned, the non-uniform penetration of the solution in concrete samples can be improved by capturing radiographs from multiple angles to get a larger number of sample investigations. This section focuses on determining the least number of angles to find a reliable analysis of a concrete

sample to obtain an accurate D_{ic}. These concrete cores were imaged from nine different angles. The data analysis considers an 18mm strip width.

This analysis assumes that capturing images from nine angles will produce the most precise outcome and that there is a lower number of angles r that can give an equivalent accuracy level. First, the number of possible permutations is calculated as:

$$\binom{9}{r} = \frac{9!}{r!\,(9-r)!} \tag{2}$$

Next, the sum of the squared errors (SSE) is calculated to demonstrate the extent of error that may arise if 'r' angles are randomly selected while assuming the nine angles as the most accurate measurements available. This analysis aims to assess the impact of such a selection on overall accuracy.

Then, an ANOVA test is run to understand any statistically significant difference between the errors based on the number of selected angles. Finally, by running a Tukey test, the statistical analysis shows how many angles are enough for accurate results.

Subsequently, an analysis of variance (ANOVA) test is conducted to evaluate whether a statistically significant difference in errors exists based on the number of selected angles. This test aims to provide insights into the potential variations in accuracy among different angle selections. A Tukey test is performed to further deepen the understanding and determine the number of angles required to achieve accurate results, as the statistical analysis determines.

The null hypothesis evaluates SSE's equality (Sum of Squared Errors) for various angle combinations. The Tukey test calculates the corresponding p-value for the below scenario.

When the SSE of the D_{ic} results is equal for images taken from i and i+1 angles, where "i" can change from 1 to 9, then this will determine the minimum number of angles that can be used to find a statistically equivalent value to the result that considers all nine angles. A p-value greater than 0.05 indicates a failure to reject the null hypothesis or a statistically significant comparison to the result that uses nine angles.

TABLE 6 presents the findings of the Tukey test conducted on the D_{ic} from 27 different concrete mixtures. Among these mixtures, capturing photographs from either four or five angles yields results comparable to those obtained from all nine angles. To simplify this, it is recommended to use five angles with all radiographs taken at least 40^{o} apart.

TABLE 6 Tukey Test Results

Fly ash type	Fly ash replacement	Age	The lowest number of angles that failed to reject the Null Hypothesis	p-value
OPC	20%	45	5	0.604
		1100	-	-
C5	20%	45	5	0.496
		1100	5	0.406
C7	20%	45	5	0.430
		1100	5	0.701
C14	20%	45	5	0.458
		1100	5	0.678
C15	20%	45	5	0.682
		1100	5	0.680
C20	20%	45	4	0.079
		1100	4	0.120
F5	20%	45	4	0.313
		1100	5	0.316
F6	20%	45	5	0.400
		1100	5	0.414
C2	40%	45	5	0.286
		1100	4	0.078
C4	40%	45	4	0.168
		1100	4	0.171
C14	40%	45	5	0.443
		1100	4	0.090
C15	40%	45	4	0.081
		1100	5	0.560
F1	40%	45	5	0.220
		1100	5	0.193
F11	40%	45	4	0.064
		1100	5	0.389

Practical implications

This study provides valuable insights into the effective utilization of X-ray radiography for calculating concrete samples' $D_{ic.}$ This research's most impactful finding is that D_{ic} measurements are feasible for inhomogeneous materials like concrete, even with non-uniform diffusion, provided that the sample can be radiographed with at least 40^{o} between angles with an 18 mm analysis width. If these parameters are used, then the average coefficient of variation is expected to be 27%. This also shows that the geometric correction factor developed for a cylindrical sample can be used to accurately estimate the D_{ic}.

Another important finding is that by using all of these parameters, the analysis is not sensitive to the aggregate size or location. It should be noted that all cores contained both mortar and aggregated at each location along the depth. This means that no core contained only aggregate at a given depth. This can be determined by visually inspecting the core after drilling.

Develop the accelerated test method

This task focuses on investigating the use of an accelerated version of the test method. This is an exploratory effort to see if the length of the test can be shortened by driving the ions through the sample with a voltage differential. Additional details of the materials used are included in a manuscript under preparation for submission to a peer-reviewed journal.

Sample preparation

Eight cores with a diameter of 19.05mm (3/4 inch) and a length of approximately 35mm were taken from concrete cylinders. Four cores were used for the non-accelerated test and four for the accelerated test. This created 208 concrete cores for testing.

The cores were vacuum-saturated at 37mm Hg ± 5mm Hg for 2 hours. This was done to fill all available pores with water. Then, concrete cores stayed in a sealed environment for 24 hours so that the large pores could empty.

Electrical migration test

The accelerated test measures the migration of ions in response to an external electrical field. By applying a voltage differential along the axis of the specimen, the test expedites the movement of ions from regions of high concentration to those with lower concentration.

The sample preparation process for the accelerated test follows the same steps as the non-accelerated test method. However, in this test, a layer of wax is applied to cover all sample surfaces except the top and bottom surfaces. Initially, radiographs are captured from nine different sides of the samples. Next, the

bottom surface of the sample is immersed in the anolyte solution, which consists of a 0.3 mol/L sodium hydroxide (NaOH) concentration. Then, a funnel is securely positioned on the top surface of the sample and filled with a catholyte solution containing 0.6 mol/L potassium iodide (KI). A voltage differential of 24 volts is then applied to the solutions, with the KI solution connected to the negative terminal and the NaOH solution connected to the positive terminal. An overview of the test method is shown in FIGURE 25.

The catholyte solution is 0.6 mol/L potassium iodide to provide suitable contrast between the paste and solution in X-ray radiography. In alignment with the methodology outlined in NT Build 492 (12), a 0.3 mol/L NaOH solution is selected as the anolyte. It is essential to record the average initial and final temperatures of the anolyte solution for each mixture, as these measurements are important in the test procedure. The accelerated test connects a power supply of 24V (±0.1 V) to catholyte and anolyte solutions. The selection of the 24 V voltage setting is derived from a study by Chinag et al. (13), which involved a comparative analysis between the salt ponding test and the accelerated migration test. This voltage is used to drive the iodide through the concrete. Applying the voltage differential initiates the migration of ions toward regions with an opposite charge. This phenomenon results in the movement of positive ions towards areas of negative charge and vice versa.

This study measured the D_{ic} of the samples after applying a voltage differential for 6, 8, 10, and 12 hours. Measuring the D_{ic} at these different periods allowed the accelerated coefficients to be compared to the non-accelerated testing and determine satisfactory correlations. The time period that shows the best correlation at the lowest time will be determined to be the best.

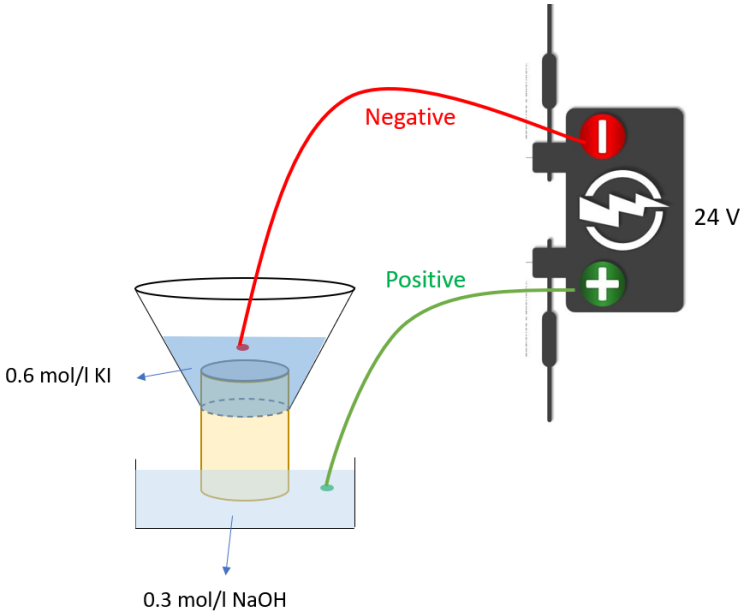

FIGURE 25 A schematic representation of the accelerated test

After a specific test duration, radiographs are taken from the same nine angles. The concentration profile is obtained using the same methodology described for the non-accelerated test.

According to NT Build 492, the non-steady-state migration coefficient (D_{nssm}) is calculated using the equation below:

$$D_{nssm} = \frac{RT}{ZFE} \times \frac{x_d - \alpha\sqrt{x_d}}{t} \quad (2)$$

Where:

$$E = \frac{U - 2}{L} \quad (3)$$

$$\alpha = 2\sqrt{\frac{RT}{ZFE}} \times erf^{-1}\left(1 - \frac{2c_d}{c_0}\right) \quad (4)$$

D_{nssm}: non-steady-state migration coefficient, $m\text{^}2/s$;

Z: Absolute value of ion valence, for iodide, Z=1.

F: Faraday constant, $F = 9.648 \times 10^4\ J/((V.mol)\ )$;

U: Absolute value of the applied voltage, which is 24 V.

R: gas constant, $R = 8.314\ J/(K.mol)$;

T: Average value of the initial and final temperature in the anolyte solution, K;

L: Thickness of the sample, m.

t: Test duration, seconds.

erf^{-1}: inverse of the error function.

c_d: A concentration value corresponding to penetration depth (%Wt. Paste)c_0: The iodide surface concentration (%Wt. Paste).

x_d: The average value of the penetration depths, m. It is the depth on the concentration profile at which the concentration equals c_d.

This study uses concentration profiles to estimate the penetration depth. Three variables are used to represent this: the initial concentration is known as c_0, the threshold used to determine the depth of concentration is called c_d, and the depth of penetration that corresponds to the concentration c_d is known as the penetration depth. FIGURE 26 shows the c_d, c_0, and penetration depth. To compare the results between the accelerated and non-accelerated testing, this study uses various values for c_d, including 0.5%, 0.75%, 1%, 1.25%, and 1.5% by weight of paste. Typically, c_0 is estimated to be within the range of 3.5% to 4.5% of the weight of the paste, as these are typical values in a non-accelerated test. This study aims to calculate the D_{nnsm} by considering a range of values for c_d and c_0 to find a value of D_{nnsm} that is close to D_{ic}.

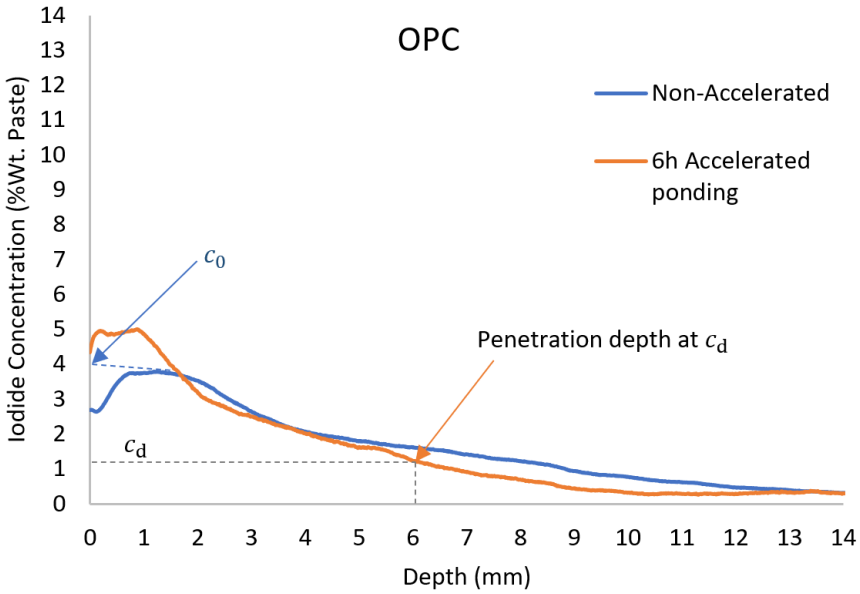

FIGURE 26 OPC concentration profile for Non-accelerated and Accelerated tests presenting the corresponding c_d, c_0, and penetration depth values.

A linear regression model is applied to both the non-accelerated and accelerated data, considering various c_0 and c_d values. The regression model is represented by the equation below:

$$\beta = \frac{D_{ic}(Non-accelerated)}{D_{nnsm}(Accelerated)} \quad (5)$$

The coefficient β is a comparison factor between the accelerated and non-accelerated D_{ic} results. If β = 1, then there is perfect agreement. If β > 1, then the non-accelerated D_{ic} is greater, and if β < 1, then the accelerated results are greater.

Comparing the accelerated and non-accelerated results

TABLE 7, TABLE 8, TABLE 9, TABLE 10, shows the R-square and β values for different c_0 and c_d values. The β values were subjected to a statistical comparison with 1.000 using a t-test. Any β values not significantly different from 1.000 were denoted with an asterisk in the respective tables.

TABLE 7 to TABLE 10 show that the R square values exceed 0.9 in most cases. **This shows that the accelerated test in as little as 6 h can provide comparable results to a non-accelerated test that takes 28 days.** This is an important achievement and could be a significant advancement in the ability to rapidly measure the D_{ic} of different samples.

TABLE 7 shows that with a 6 h accelerated test and using c_d = 1.25 and c_0 = 3.5% by weight of the paste, the β value is 1, indicating that D_{ic} and D_{nnsm} are approximately equal, with an R square of 0.96.

These findings show an accelerated ponding period of 6 hours, and using X-ray radiography to calculate the concentration profile can provide statistically equal results as a non-accelerated test.

FIGURE 27 compares the non-accelerated and accelerated results after 6h with $c_d = 1.25$ and $c_0 = 3.5\%$ by weight of the paste. It shows a good correlation between D_{ic} and D_{nnsm} after 6 hours of accelerated ponding regardless of age, fly ash type, and fly ash replacement.

As mentioned previously, this study uses 45-day and 1100-day-old samples to compare how mature samples respond to the accelerated test. Table 7 shows the D_{ic} and D_{nnsm} values used for plotting FIGURE 27. Based on the data in TABLE 7, it is noteworthy that even for mature samples aged 1100 days, a notable correlation is observed between D_{ic} and D_{nnsm} for 20% fly ash replacement after 6 hours of ponding.

However, when examining four mature mixes, which included 40% fly ash replacement, the accelerated test couldn't establish a similar D_{nnsm}. These four data points were outliers, showing an absolute standard deviation of residuals higher than 2 in the linear regression table. This deviation seems to be because the material's D_{ic} is $< 1 \times 10^{-12} \left(\frac{m^2}{s}\right)$. As a result, the accelerated test may not be able to provide accurate results when the D_{ic} is this low; however, additional testing is required to confirm this. These outliers are visually represented by red dots in FIGURE 27 and marked as asterisks in TABLE 7. It should be noted that the models used to predict D_{ic} based on D_{nnsm} in TABLE 7, TABLE 8, TABLE 9, and TABLE 10 were developed without considering these outlier data points.

TABLE 7 The Linear Regression Results After 6 Hours of Accelerated Ponding for Different c_0 And c_d Values Without Considering Outliers, Number of The Samples: 92 Samples.

		$c_d = 0.5$ %Wt. Paste	$c_d = 0.75$ %Wt. Paste	$c_d = 1$ %Wt. Paste	$c_d = 1.25$ %Wt. Paste	$c_d = 1.5$ %Wt. Paste
$c_0 = 3.5$ %Wt. Paste	β	1.96	1.43	1.19	1.00*	0.91*
	R^2	0.85	0.92	0.95	0.96	0.95
$c_0 = 4$ %Wt. Paste	β	1.96	1.41	1.18	0.98*	0.89
	R^2	0.85	0.92	0.95	0.96	0.95
$c_0 = 4.5$ %Wt. Paste	β	1.92	1.39	1.16	0.96*	0.87
	R^2	0.85	0.92	0.95	0.96	0.95

* The value is not statistically different from 1.00

TABLE 8 The Linear Regression Results After 8 Hours of Accelerated Ponding For Different c_0 And c_d Values, Without Considering Outliers, The Number of Samples: 52 Samples.

		$c_d = 0.5$ %Wt. Paste	$c_d = 0.75$ %Wt. Paste	$c_d = 1$ %Wt. Paste	$c_d = 1.25$ %Wt. Paste	$c_d = 1.5$ %Wt. Paste
$c_0 = 3.5$ %Wt. Paste	β	1.47	1.23	1.09*	0.99*	0.91*
	R^2	0.93	0.96	0.96	0.95	0.94
$c_0 = 4$ %Wt. Paste	β	1.45	1.25	1.07*	0.97*	0.88*
	R^2	0.94	0.94	0.96	0.95	0.95
$c_0 = 4.5$ %Wt. Paste	β	1.64	1.22	1.06*	0.96*	0.86*
	R^2	0.87	0.94	0.95	0.95	0.95

* The value is not statistically different from 1.00

TABLE 9 The Linear Regression Results After 10 Hours of Accelerated Ponding For Different c_0 and c_d Values, Without Considering Outliers, The Number of Samples: 52 Samples

		$c_d = 0.5$ %Wt. Paste	$c_d = 0.75$ %Wt. Paste	$c_d = 1$ %Wt. Paste	$c_d = 1.25$ %Wt. Paste	$c_d = 1.5$ %Wt. Paste
$c_0 = 3.5$ %Wt. Paste	β	1.56	1.33	1.04*	0.93*	0.89
	R^2	0.86	0.89	0.94	0.94	0.92
$c_0 = 4$ %Wt. Paste	β	1.51	1.31	1.03*	0.92*	1.07*
	R^2	0.89	0.89	0.94	0.94	0.93
$c_0 = 4.5$ %Wt. Paste	β	1.49	1.31	1.03*	0.91*	0.85*
	R^2	0.89	0.89	0.93	0.93	0.93

* The value is not statistically different from 1.00

TABLE 10 The Linear Regression Results After 12 Hours of Accelerated Ponding For Different c_0 And c_d Values, Without Considering Outliers, The Number of Samples: 20 Samples.

		$c_d = 0.5$ %Wt. Paste	$c_d = 0.75$ %Wt. Paste	$c_d = 1$ %Wt. Paste	$c_d = 1.25$ %Wt. Paste	$c_d = 1.5$ %Wt. Paste
$c_0 = 3.5$ %Wt. Paste	β	1.72	1.45	1.22	0.94*	0.8*
	R^2	0.87	0.85	0.90	0.85	0.91
$c_0 = 4$ %Wt. Paste	β	1.72	1.43	1.20	0.93*	0.79
	R^2	0.90	0.85	0.90	0.88	0.90
$c_0 = 4.5$ %Wt. Paste	β	1.69	1.43	1.19	0.92*	0.77
	R^2	0.90	0.85	0.90	0.88	0.90

* The value is not statistically different from 1.00

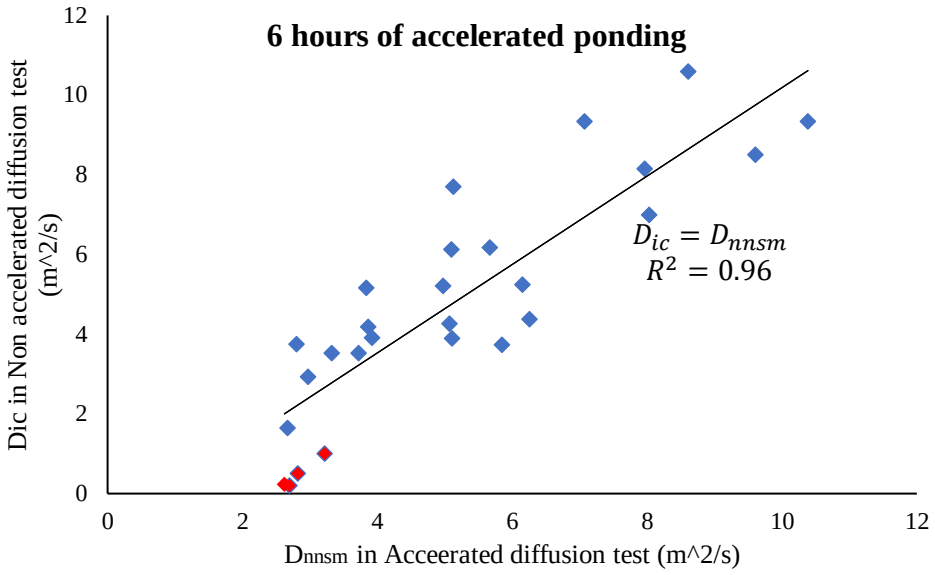

Note: The red dots in this figure show outlier data.

FIGURE 27 Correlation diagram: Comparison between 28 d of non-accelerated D_{ic} data (Y-axis) and D_{nnsm} after 6 hours of accelerated ponding (X-axis) c_d=1.25 and c_0=3.5% weight of paste.

Practical implications

This work shows that accelerated testing in 6 h with the right testing parameters can provide data comparable to non-accelerated testing that takes 28 d of testing for samples that have a D_{ic} > 1×10^{-12} $\left(\frac{m^2}{s}\right)$. This means the test can be used on a wide variety of samples as the only materials with diffusion coefficients this low were from mixtures that contained 40% fly ash replacement after 1100 days of curing.

The ability to obtain diffusion coefficients that are this accurate with only 6 hours of testing time is quite useful and can make this test even easier to implement. While these findings are important, testing is needed with a wider variety of materials and diffusion coefficients. This work focused on mixtures with a narrow range of w/cm and SCM replacement. The parameters chosen in this work for c_d and c_0 may need to be adjusted for a wider range of materials. This is an area of future work.

Evaluate the repeatability of the test

This section provides a written description of the recommended test method. The test has been written in a format that makes it easily adapted for a standard test method. This description focuses on the non-

accelerated version of the test because more work is needed with a wider range of materials and samples with the accelerated test method to determine the correct parameters to use.

Overview of the test method

This test uses X-ray radiography to visualize the penetration of the outside salts inside paste, mortar, or concrete. This can be used to calculate the diffusion coefficient (D_{ic}). The method is called Checking Ion Penetration (CHIP). CHIP is a cost-effective dental X-ray equipment adapted to rapidly complete transmission X-ray microscopy (TXM) equivalent measurements. A schematic view of CHIP is shown in FIGURE 28, and TABLE 11 shows the instrument settings for CHIP.

These radiographs are used to determine the D_{ic} of the sample by taking time-resolved images of tracers penetrating from the surface of the top surface of the sample. First, the CHIP takes X-ray radiographs of the sample from five angles prior to a tracer being added to the surface. These are the initial images that will be used to compare to the images after the samples have been ponded with a tracer. Next, the samples are coated with wax and then ponded with a 0.6 mol/l potassium iodide (KI) solution for 28 days. The solution on top of the samples was changed every five days to provide samples with a constant KI concentration. After 28 days, the radiographs are taken with the CHIP at the same angles used to take the initial images. These images are compared to determine the concentration of the KI over the depth.

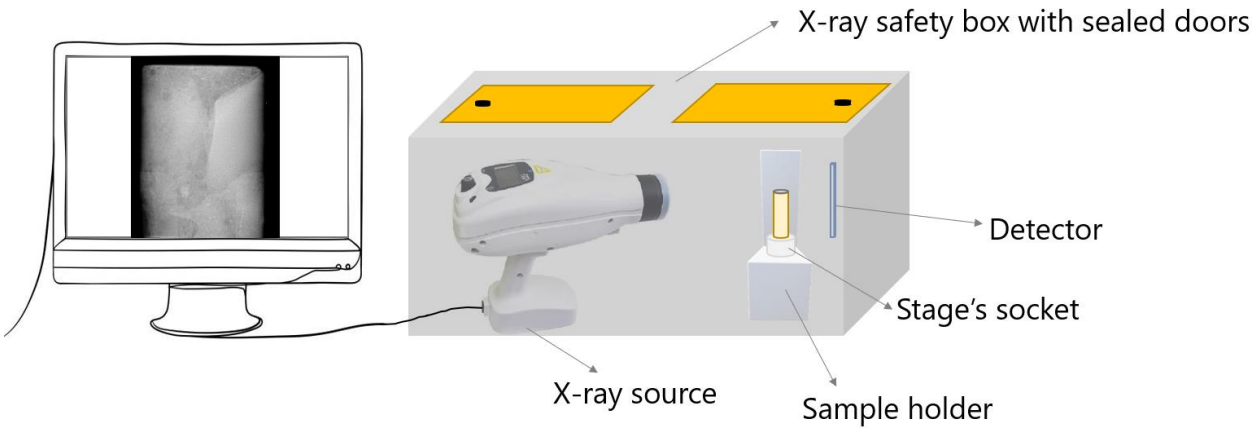

FIGURE 28 Schematic view of Checking Ion Penetration (CHIP) X-ray instrument

TABLE 11 The Instrument Setting Used in CHIP

Parameter	Pixel Size	Voltage	Current	Filter	Exposure time
Value	15 μm	120 KeV	7000 μA	1.5 mm Al	8 second

This work used KI for several reasons. First, the high electron density of KI makes it strongly X-ray attenuating. This property makes KI an excellent tracer for the fluid transport study of concrete with X-rays. As the tracer penetrates the material, it is possible to see the corresponding changes in X-ray absorption because it provides a suitable contrast between the paste and solution. Second, KI is widely available, and iodide and chloride ions are similar in size. Third, Khanzadeh. et al. show that the diffusion profile for iodide and chloride was comparable (14).

CHIP data analysis

As mentioned previously, CHIP captures radiographs of the concrete samples twice: once before (initial image) and once after ponding with a 0.6 mol/l KI solution for 28 days (28-day image). These radiographs are turned into grayscale images where each pixel is assigned a gray value ranging from 0 to 254, indicating its brightness level. A pixel with a value of 0 represents black, while a pixel with a value of 254 represents white.

The initial step in image analysis involves calculating the average gray value for each depth within the image. The intensity of an X-ray beam decreases in proportion to the depth of penetration or thickness of the material. For instance, the edges of a cylinder core allow more energy to pass through since they have a smaller thickness compared to the center.

To address this issue, a thickness correction factor is introduced. This factor is defined in Equation 6:

$$\text{Thickness correction factor} = \frac{\text{Avg gray value of the center pixel}}{\text{Avg gray value on width n}} \quad 0 < n < x \qquad (6)$$

The term 'Avg gray value of the center' refers to the average gray value over height observed at the center of the sample. On the other hand, the 'Avg gray value on width n' represents the average gray value over height observed at any location across the width of the sample. The width 'x' for concrete samples ranges from 0 to 18 mm, while for paste or mortar samples, it ranges from 0 to 8 mm.

Next, the average gray value of the 28-day image is subtracted from the initial image. The subtracted image provides insight into how the solution penetrates through the sample (FIGURE 29).

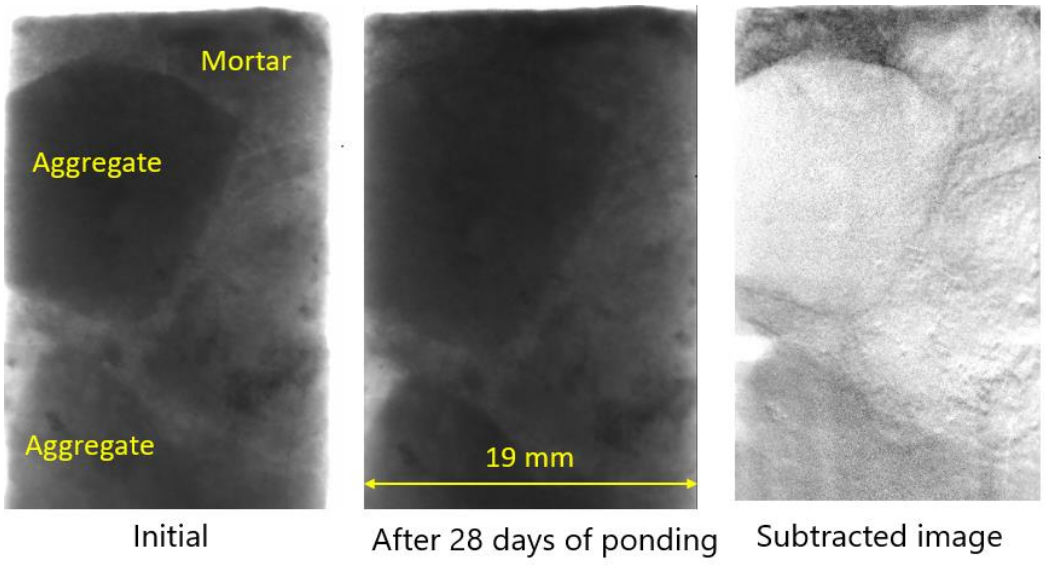

FIGURE 29 X-ray photographs before and after ponding with the solution

The average gray values before and after ponding are used in Beer-Lambert law (Equation 7) (6,7) to calculate attenuation changes in depth.

$$(\Delta\mu)_x = ln(I_{ref})_x - ln(I_t)_x \quad (7)$$

Where $(I_{ref})_x$ is the gray value in the initial image and $(I_t)_x$ is a 28-day gray value in the same depth and $(\Delta\mu)_x$ is the change in attenuation. The third step is determining the iodide concentration profile and calculating the diffusion coefficient.

Samples with known KI concentrations in their mixture were prepared to generate a calibration curve. Using CHIP, radiographs of these samples were collected to correlate the resulting gray value to the concentration of KI. These known concentration values were then employed to establish a calibration curve that converts attenuation values to concentrations.

In most practical diffusion scenarios, the diffusion flux and concentration gradient are time-varying for concrete; this makes the diffusion a non-steady-state condition. Fick's second law (Equation 8) describes the diffusion process in a single direction for a non-steady-state condition.

$$\frac{\partial C}{\partial t} = D_{ic}\frac{\partial^2 C}{\partial x^2} \quad (8)$$

Where:

D_{ic} :Diffusion coefficient

C : Concentration

x : Depth

t : Time

Equation 9 is a non-linear regression model based on Fick's second law. It is applied to concentration data points to determine the diffusion coefficient.

$$C_{(x,t)} = C_s\left(1 - \text{erf}\left(\frac{x}{2\sqrt{D_{ic}t}}\right)\right) \quad (9)$$

Where $C_{(x,t)}$ is the concentration in depth x from the top surface at time t, and erf is defined as an error function.

The higher the R-square value associated with equation 9 in describing the data points within the concentration profile, the stronger the correlation observed between iodide penetration and the occurrence of non-steady state diffusion.

By using these settings, it has been shown that R-square values greater than 90% are typical. A single operator precision leads to a coefficient of variation of 20% for paste samples with an analysis width of 8 mm and for at least two investigated angles that are at least 40^o apart and 27% for concrete samples with an analysis width of 18 mm for at least 5 investigated angles that are > 40^o apart.

Plans for Implementation

The CHIP has been successfully used in several case studies to learn more about the quality and performance of concrete mixtures. Further, the machine has been made more practical and easier to use. The next step would be to work with DOTs to help them build CHIPs so that they can use them or so that they can use a contractor to test samples that they create. Three potential groups to start using the CHIP are Oklahoma DOT, Massachusetts DOT, and the FHWA Mobile Concrete Trailer. The Mobile Concrete Trailer provided a support letter at the start of the project. Oklahoma DOT has worked with Oklahoma State University to use the CHIP to investigate several possible issues with their concrete mixtures, and Massachusetts DOT has supplied materials to be investigated with the CHIP. This shows that DOTs are interested in the use of the equipment.

This exposure from the FHWA mobile lab and other DOTs will help others learn about the CHIP, and it will also help to continue to gather data from a number of different projects. These results will then be shared with other SHAs, FHWA, and AASHTO through personal contacts, sharing the results at conferences and YouTube videos. After obtaining the interest of owners, efforts will be made to contact testing companies and show them the usefulness of the CHIP.

Ultimately, the CHIP will be marketed through Gilson, the largest construction testing equipment manufacturer in North America. The research team already has a relationship with Gilson and a signed non-disclosure agreement to collaborate on developing concrete testing equipment. After sufficient demand is produced, the product will be made commercially available.

Conclusions

In summary, the research team has completed all of the tasks outlined in the project. This includes building an improved sample holder for the CHIP, improving the computer algorithms, using the equipment for three case studies, improving the accuracy of the method, investigating an accelerated version of the test, and providing an outline of the test method. The following findings have come from this work:

The CHIP was used to complete three different case studies to quantify the impact of wet curing, the effectiveness of silanes, and also quantify the ability to make long-term changes in the D_{ic} of concrete.

When samples were investigated with a strip width of 18 mm and from at least 5 angles, the reliability of concrete measurements was improved, and the coefficient of variation with a single operator was found to be 27%. The coefficient of variation of paste was found to be 20%. These samples were ponded with KI solution for 28 days.

An accelerated version of the test was developed that reduced the ponding time from 28 days to only 6h by applying 24V during ponding. This accelerated test was not able to accurately measure samples with a $D_{ic} < 1 \times 10^{-12} \left(\frac{m^2}{s}\right)$. It should be noted that these samples are not common, but more testing is needed to see if this test can be used on a wide number of samples.

An outline of the recommended test method is provided. This provides a useful starting place to standardize the test method. A draft of an AASHTO Test Method is provided in the appendix.

References

1. Neville AM. Properties of concrete. Vol. 4. London; 1995.

2. Safiuddin M, Raman SN, Zain M. Effect of Different Curing Methods on the Properties of Microsilica Concrete. Australian Journal of Basic and Applied Sciences. 2007 Jan 1;1:87–95.

3. Gowripalan N. Effect of Curing on Durability. CI. 1990 Feb 1;12(2):47–54.

4. Zhutovsky S, Kovler K. Effect of internal curing on durability-related properties of high performance concrete. Cement and Concrete Research. 2012 Jan 1;42(1):20–6.

5. Kosmatka S, Wilson M. Design and Control of Concrete Mixtures. 2011.

6. Ramezanianpour AA, Malhotra VM. Effect of curing on the compressive strength, resistance to chloride-ion penetration and porosity of concretes incorporating slag, fly ash or silica fume. Cement and Concrete Composites. 1995 Jan 1;17(2):125–33.

7. Montgomery FR, Basheer P a. M, Long AE. Influence of Curing Conditions on the Durability Related Properties of Near Surface Concrete and Cement Mortars. SP. 1992 Mar 1;131:127–38.

8. Zain MF, Matsufuji Y. The influence of curing methods on the physical properties of high strength concrete exposed to medium temperature (20–50 ºC). Proceedings of the Fifth International Conference on Concrete Engineering and Technology, Kuala Lumpur, Malaysia. 1997;

9. Zain M, Safiuddin M, Yusof K. Influence of different curing conditions on strength and durability of high-performance concrete. 2000.

10. ACI Committee 305. 1-06. Specification for Hot Weather Concreting. American Concrete Institute Farmington Hills, MI.; 2007.

11. Chen L. Novel Methods of Quantifying Curing Influence and Freeze Thaw Cycles in the Field [Internet] [Ph.D.]. [United States -- Oklahoma]: Oklahoma State University; 2022 [cited 2023 Oct 5]. Available from: https://www.proquest.com/docview/2759102006/abstract/D56040D537904FACPQ/1

12. NT BUILD 492, Chloride Migration Coefficient From Non-Steady-State Migration Experiments. NORDTEST, Finland,; 1999.

13. Chiang CT, Yang CC. Relation between the diffusion characteristic of concrete from salt ponding test and accelerated chloride migration test. Materials Chemistry and Physics. 2007 Dec 15;106(2):240–6.

14. Khanzadeh Moradllo M, Ley MT. Comparing ion diffusion in alternative cementitious materials in real time by using non-destructive X-ray imaging. Cement and Concrete Composites. 2017 Sep 1;82:67–79.

Appendix: Research Results

Sidebar Info Program Steering Committee: NCHRP IDEA Program Committee
Month and Year: August, 2023
Title: Measuring Concrete Permeability with the CHIP
Project Number: IDEA Project NCHRP-232
Start Date: July 1, 2021
Completion Date: October 1, 2023
Product Category: IDEA Project
Principal Investigator: M. Tyler Ley
Title: Regents Professor
E-Mail: tyler.ley@okstate.edu
Phone: 405-744-5257

TITLE: Measuring Concrete Permeability with the CHIP

SUBHEAD: This work improved a device to measure the permeability of concrete and created case studies for State Highway Associations.

Answer the following questions in 550–650 words.

WHAT WAS THE NEED?

Concrete infrastructure is a significant investment for State Highway Agencies (SHAs). Because of this, these concrete structures must have a long service life. The permeability of concrete is critical in the durability of concrete. This work improves an existing device called the CHIP (**ch**ecking **i**on **p**enetration). The CHIP can determine the permeability of concrete with a non-destructive, practical, fast, safe, and easy to use. This device uses X-ray to image the penetration of outside salts into the concrete. The CHIP can be used to evaluate the permeability of concrete during mixture designs, construction, or for concrete structures in service. This ability to rapidly and economically determine the permeability of concrete and predict the service life is a powerful tool for SHAs.

WHAT WAS OUR GOAL?

Our goal was to create a new tool for SHAs to measure the quality of their concrete during mixture design evaluation, construction, or when planning the maintenance for existing structures.

WHAT DID WE DO?

This work created a new state that allowed larger samples and was more accurate, improved the computer software used to complete the test, created a stage that allowed the sample to be investigated from a larger number of angles that increased the accuracy, accelerated the test method by using electrical migration. This work also completed three case studies with the instrument to investigate surface coatings, the effectiveness of different types of fly ash, and the impact of different delays in wet curing.

WHAT WAS THE OUTCOME?

The created stage is 4x more accurate and allowed larger samples, the improved computer software reduced operator time by 3x, the variability of the results of concrete samples was decreased by 90%, and the accelerated test method reduced the testing time from 28 days to 6 hours. In all three case studies the CHIP provided useful insights into the effectiveness of surface coatings for concrete, the effectiveness of different types of fly ash in a concrete mixtures, and the impact of delays in wet curing for concrete.

WHAT IS THE BENEFIT?

By using the CHIP, SHAs will make better decisions about accepting and rejecting concrete mixture and make better decisions on how to maintain concrete structures that are in service.

LEARN MORE: - <Please provide a link to the final report.>

IMAGES

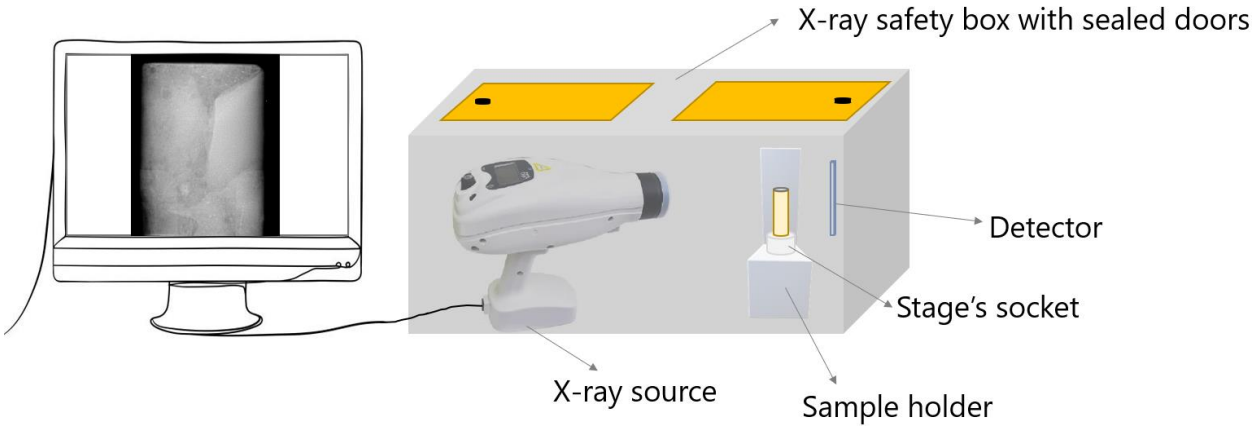

Figure A1 A Schematic view of Checking Ion Penetration (CHIP) X-ray instrument.

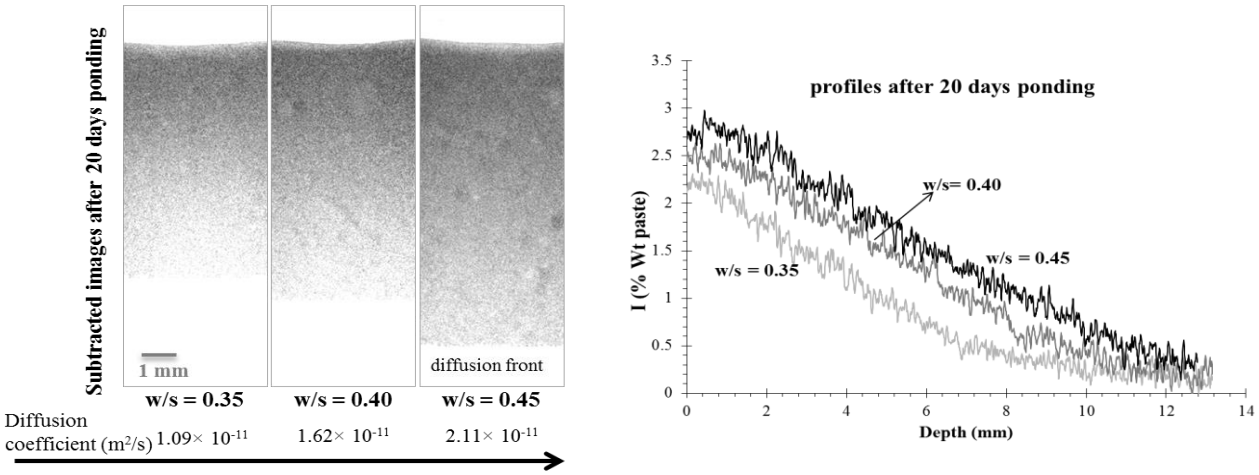

(a) (b)

Figure A2 (a) ion penetration and (b) ion concentration profile of three mixtures with different w/cm and diffusion coefficients.

Appendix: AASHTO Provisional Test Method Rough Draft